

# Predicting Chemical Reaction Equilibrium in Dilute Solutions by Atomistic Simulation: Application to CO<sub>2</sub> Reactive Absorption in Aqueous Primary Alkanolamine Solutions

Javad Noroozi<sup>\*,†</sup> and William R. Smith<sup>\*,‡,¶</sup>

<sup>†</sup>*Department of Chemical Engineering, University of Waterloo, Waterloo ON N2L 3G1,  
Canada*

<sup>‡</sup>*Department of Mathematics and Statistics, University of Guelph, Guelph ON N1G 2W1,  
Canada*

<sup>¶</sup>*Faculty of Science, University of Ontario Institute of Technology, Oshawa ON L1H 7K4,  
Canada*

E-mail: jnoroozi@uwaterloo.ca; bilsmith@uoguelph.ca

Final Version 4, July 15, 2020

## Abstract

We present a general atomistic simulation framework for efficient reactive equilibrium calculations in dilute solutions, and its application to CO<sub>2</sub> reactive absorption in aqueous alkanolamine solutions. No experimental data of any kind for the solvents is required and no empirical adjustments are required for its implementation. This hybrid methodology involves calculating the required reaction equilibrium constants by combining high-level quantum chemical calculations of ideal-gas standard reaction Gibbs energies ( $\Delta G^0$ ) with conventional free energy calculations for transfer of the molecular species from the ideal gas to infinite dilution in the solvent (*i.e.*, their solvation free energies). For the solvation free energy calculations, we use explicit solvent molecular dynamics simulations with the General AMBER Force Field (GAFF). The resulting equilibrium constants are then coupled with a macroscopic Henry–Law–based ideal solution model to calculate the solution speciation and the CO<sub>2</sub> partial pressure,  $P_{\text{CO}_2}$ . We show results for seven primary amines: monoethanolamine (MEA), 2-amino-2-methylpropanol (AMP), 1-amino-2-propanol (1-AP), 2-amino-2-methyl-1,3-propanediol (AMPD), 2-aminopropane-1,3-diol (SAPD), 2-(2-aminoethoxy)ethanol (2-AEE) or diglycolamine (DGA), and 2-amino-1-propanol (2-AP). Experimental speciation and  $P_{\text{CO}_2}$  data for some of these is available, with which we validate our methodology. We predict new results for others in cases when such data is unavailable, and provide explanations for the experimental inability to detect carbamate species in some cases. Our results for the  $pK$  value of the carbamate reversion reaction are within the chemical accuracy limit of  $218.506/T$  in comparison with experiment when such data exist, which at 298.15 K corresponds to 0.73  $pK$  units. We argue that the precision of our  $pK$  predictions in general is comparable to that which can be obtained from conventional experimental methodologies for these quantities. Our results suggest that the presented molecular simulation methodology may provide a robust and cost-efficient tool for solvent screening in the design of post-combustion CO<sub>2</sub> capture processes.

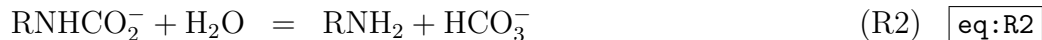
# 1 Introduction

Increasing atmospheric concentrations of CO<sub>2</sub> and other greenhouse gases and their consequent environmental effects have prompted a large body of research probing the CO<sub>2</sub> capturing properties of adsorbing materials and absorbing chemical solvents. Carbon capture and storage (CCS) is considered to be one of the most viable short term options for reducing global carbon emissions.<sup>[[Kumoro2018](#),[Song2018](#)]</sup> Chemical absorption using aqueous alkanolamine solutions currently being used in industry are considered one of the most mature options for large-scale CO<sub>2</sub> capture.<sup>[[dutcher2015amine](#)]</sup> However, the capture process suffers from several drawbacks, including high solvent regeneration energy costs, both due to parasitic energy losses due to the high latent heat of the water co-solvent, and the formation of the thermally stable carbamates, which also result in poor cyclic capacity.<sup>[[hartono2017screening](#)]</sup> In order to circumvent these problems, various alternative solvents, such as non-aqueous solvents,<sup>[[barzagli2013efficiency](#)]</sup> lipophilic amines<sup>[[gittang2012improvement](#)]</sup> and phase changing compounds<sup>[[pinto2014evaluation](#)]</sup> have been recently considered. Unravelling the effects of different functional groups in the amine structures on their behaviour is crucial for the design of improved alkanolamine-based CO<sub>2</sub> capturing solvents. For example, heavily hindered alkanolamines have been shown to reversibly absorb CO<sub>2</sub> in an equimolar ratio and CO<sub>2</sub> can completely be desorbed at relatively low regeneration temperatures.<sup>[[choi2014co2](#)]</sup>

The CO<sub>2</sub> capturing properties of the absorbent are a consequence of the kinetic and chemical reaction equilibrium properties resulting from the CO<sub>2</sub> dissolution, and the equilibrium composition of CO<sub>2</sub> in the solvent is an important tool for solvent screening. In the case of primary and secondary amines, CO<sub>2</sub> is absorbed primarily in the form of carbamate (RNHCO<sub>2</sub><sup>-</sup>), bicarbonate (HCO<sub>3</sub><sup>-</sup>) and carbonate (CO<sub>3</sub><sup>-2</sup>) species, in coexistence with protonated amine (RNH<sub>3</sub><sup>+</sup>), amine (RNH<sub>2</sub>), water and its ionization products (OH<sup>-</sup> and H<sub>3</sub>O<sup>+</sup> or H<sup>+</sup>), and free CO<sub>2</sub> in the solution.

The set of linearly independent chemical equations used to model chemical reaction equilibrium is governed only by the requirement that their number is given by  $R = N - \text{rank}(\mathbf{A})$ , where  $N$  is the number of species and  $\mathbf{A}$  is the species formula matrix,<sup>[[Smith1991b](#)]</sup> the following stoi-

chiometry provides a convenient basis for describing the reaction equilibria of the indicated species in the case of primary and secondary amines.



We remark that any sets of linear combination of the above reactions may be selected based on the numerical convenience used to solve the system of non-linear equation. Tertiary amines do not form carbamates, and reactions  $\boxed{\text{eq:R1}}$  and  $\boxed{\text{eq:R2}}$  can be replaced by their sum



The equilibrium constants (or equivalently, the  $pK$  values) for reactions  $\boxed{\text{eq:R3}}$ – $\boxed{\text{eq:R6}}$  as functions of temperature are experimentally well-known. Their experimental determination for reactions  $\boxed{\text{eq:R1}}$  and  $\boxed{\text{eq:R2}}$  requires new data for each solvent. Furthermore, the equilibrium constants can only be determined indirectly from such data, by fitting to the parameters of empirically based chemical potential models or equations of state.  $pK$  values have been determined in this way by fitting to experimental potentiometric titration measurements for the carbamate reversion reaction  $\boxed{\text{eq:R2}}$ ,<sup>10</sup> and for the amine protonation reaction,<sup>10–16</sup> which is the linear combination of  $\boxed{\text{eq:R1}}$ – $\boxed{\text{eq:R2}}$ – $\boxed{\text{eq:R3}}$ .



$pK$  values have also been obtained by fitting thermodynamic models to experimental

spectroscopically obtained speciation data of CO<sub>2</sub>-loaded solutions.<sup>[mccann2011systematic](#),[fernandes2012](#)</sup> In such experimental studies, the presence of the fast proton-exchanging species (*i.e.*, CO<sub>3</sub><sup>-2</sup>/HCO<sub>3</sub><sup>-</sup> or (RNH<sub>3</sub><sup>+</sup>/RNH<sub>2</sub>) pairs) complicates the data analysis, and usually only the total concentration of the carbonate/bicarbonate pair is available and can be used in the parameter fitting. (We note in passing that the uncertainties of speciation data from NMR are much larger than those from titration measurements.)

Finally, parameters of chemical potential models and/or equations of state have been fitted to reaction models of CO<sub>2</sub> solubility data.<sup>[Deshmukh1981](#)</sup> In other cases, the reactions have been approximated by pseudo-reaction physical association models incorporated in either the SAFT<sup>[Najafloo2016](#),[Wang2018](#),[Wang2019](#),[Wang2018](#),[Wangler2018](#)</sup> or CPA<sup>[Wang2018](#),[Wangler2018](#)</sup> approaches.

Experimental screening of the vast number of potential solvent candidates is prohibitively expensive and time consuming, and more predictive and less costly computational tools offer a promising alternative and complementary approach. The ability to accurately predict the equilibrium speciation and the associated CO<sub>2</sub> partial pressure for CO<sub>2</sub>-loaded solutions of candidate solvents is one of the most important requirements, which is very challenging due to the complex chemical reaction and phase equilibria involved.

Three general approaches have been used toward this goal: combined Electronic Structure (ES) dielectric continuum solvent (DCS) models, *ab initio* MD methods, and classical force-field (CFF) methodologies. The first group includes methods based on the Conductor-like Screening Model for Realistic Solvents (COSMO-RS)<sup>[Klamt2011cosmo](#),[Gerlach2018a](#)</sup> and Solvation Models based on Density (SMD).<sup>[Marenich2009universal](#)</sup> These have been used to study reaction mechanisms and the relative stability of the carbamate product species.<sup>[Gangarapu2013carbamate](#),[Xie2014theoretical](#),[Gerlach2018](#),[Gupta2018](#)</sup> Alternative DCS methods such as the SMDx family of Cramer *et al.*,<sup>[Marenich2009universal](#)</sup> usually trained based on hydration free energy data of neutral molecules at 298.15 K, may be potentially applied to such systems; however, their extension to ionic species and to higher temperatures has not been fully tested. Whereas the deficiencies of the continuum solvation models can be partially overcome by incorporating explicit solvent molecules in the first solvation shell,<sup>[Teranishi2017](#)</sup> their application to flexible molecules

is not straightforward.<sup>[haworth2017modeling]</sup>

In the second group, Nakai *et al.*<sup>[nakai2016contrasting,Sakti2017a,Sakti2017b]</sup> used density-functional tight-binding molecular dynamics (MD) simulations to study reaction mechanisms in CO<sub>2</sub> chemical absorption and regeneration processes in aqueous amine solutions. While such approaches do not require *a priori* knowledge of the identity of product species, they require detailed geometric criteria to dynamically evaluate their chemical identity and population at each step of the MD simulation. Moreover, such *ab initio* methods have only been carried out for relatively small system sizes and scale poorly with the system size, making them highly inefficient for the high throughput CO<sub>2</sub> solvent screening task. Other *ab initio* approaches based on first principles calculations have also been developed and used for speciation predictions in reactive systems.<sup>[fetisov2016first]</sup>

CFF methodologies have been employed by the groups of Vlught *et al.*,<sup>[Balaji2015b]</sup> Maginn *et al.*,<sup>[Mullen2018b]</sup> and our group.<sup>[noroozi2019efficient,Balaji2015b]</sup> Balaji *et al.*<sup>[Balaji2015b]</sup> used the Reaction Ensemble (REMC) algorithm<sup>[Smith1994c,Johnson1994]</sup> in conjunction with fractional insertion of molecular species in a preliminary study of reaction equilibria in the MEA-CO<sub>2</sub>-H<sub>2</sub>O system. Although the REMC algorithm was incorrectly implemented (by omitting the atomization energies in the ideal-gas standard reaction free energy contribution<sup>[noroozi2019efficient]</sup>), it was fortuitously able to reasonably predict the most abundant species in the system at low to moderate CO<sub>2</sub> loadings. Mullen *et al.*<sup>[Mullen2018b]</sup> applied the REMC algorithm in conjunction with an enhanced Monte Carlo sampling approach for CO<sub>2</sub> absorption in a reactive ionic liquid. MC-based approaches for complex systems such as those involved in CO<sub>2</sub> reactive absorption suffer from the computational disadvantage of requiring special system-specific sampling moves; they also require very long computation times and/or large system sizes to deal with the concentrations of species present in small amounts. These drawbacks make the REMC approach inefficient for their use in solvent screening.

Based on a recently developed reaction equilibrium algorithm requiring only straightforward conventional CFF-based MD free energy calculations coupled with ES ideal gas phase calculations,<sup>[Smith2018b]</sup> we recently implemented<sup>[noroozi2019efficient]</sup> a general and computationally efficient reaction

equilibrium algorithm to predict CO<sub>2</sub> solubility and successfully applied it to speciation (including species present in very small concentrations) in the benchmark CO<sub>2</sub>–MEA–H<sub>2</sub>O system.

The goal of this paper is to improve and extend this CFF-based methodology and apply it to the prediction of CO<sub>2</sub> reactive absorption speciation and  $P_{\text{CO}_2}$  data as functions of loading, temperature and solvent composition for aqueous MEA and six additional primary alkanolamine systems, whose molecular structures are shown in Fig. 1. For the other amines, we compare our predictions with (often limited) experimental  $P_{\text{CO}_2}$  data, and with solution speciation data, which in some cases is unavailable experimentally.

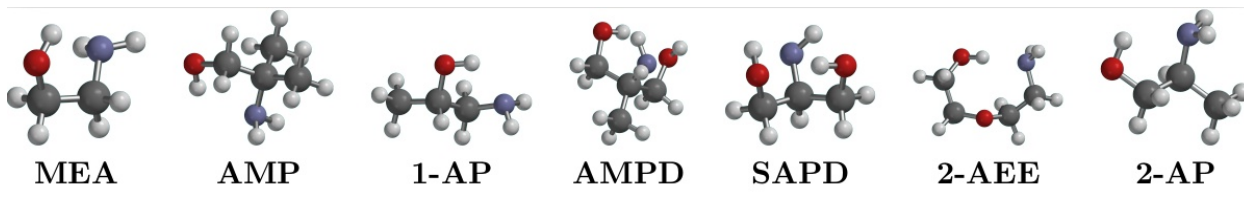


Figure 1: Molecular structures of the studied alkanolamines.

## 2 Molecular-Based Thermodynamic Methodology

The equilibrium composition of a closed chemically reacting system at specified  $(T, P)$  can be obtained by minimizing its Gibbs free energy subject to the conservation of mass and electroneutrality constraints, and implemented by calculating the solution of the  $R$  equations

$$\Delta G_j(T, P; \mathbf{x}) \equiv \sum_{i=1}^{N_s} \nu_{ij} \mu_i(T, P; \mathbf{x}) = 0; \quad j = 1, 2, \dots, R \quad (1)$$

where  $\nu_{ij}$  is the stoichiometric coefficient of species  $i$  in reaction  $j$  and  $\mathbf{x}$  represents the system composition vector. The reaction equilibrium composition can be readily accomplished by a wide range of numerical algorithms<sup>Smith1991b</sup> and chemical potential models, and we employ here a Henry–Law ideal solution model. The chemical potentials (for both solutes and solvent) in

this model are expressed as

$$\mu_i(T, P; \mathbf{m}) = \mu_i^\dagger(T; P) + RT \ln \left( \frac{m_i}{m^0} \right), i = 1, 2, \dots, N_{\text{solv}} \quad (2) \quad \text{eq:muHenry}$$

where  $T$  is the absolute temperature,  $P$  is the pressure,  $R$  is the universal gas constant, and  $\mu_i(T, P; \mathbf{m})$  is the chemical potential of species  $i$ , and  $\mathbf{m}$  is the vector of molalities.

We have previously shown<sup>Nezbeda2016a</sup> that the standard chemical potential  $\mu_i^\dagger(T; P)$  of solute species  $i$  can be calculated from molecular simulation quantities by

$$\mu_i^\dagger(T, P) = \mu_i^0(T; P^0) + RT \ln \left( \frac{RT M_{\text{solv}} m^0 \rho_{\text{solv}}^*(T, P)}{1000 P^0} \right) + \mu_i^{\text{res}, NVT, \infty}[T, \rho_{\text{solv}}^*(T, P)] \quad (3) \quad \text{eq:mudagfi}$$

where  $\mu_i^0(T; P^0)$  is the ideal gas chemical potential of species  $i$ , which can be calculated using standard expressions for the partition function of ideal-gas molecule under the harmonic oscillator rigid rotor approximation,<sup>McQuarrie2000, ochterski2000thermochemistry</sup>  $\rho_{\text{solv}}^*(T, P)$  is the density of the pure solvent (water in our case),  $M_{\text{solv}}$  is its molecular weight, and  $m^0 = 1 \text{ mol} \cdot \text{kg}^{-1}$  solvent. For a solute,  $\mu_i^{\text{res}, NVT, \infty}[T, \rho_{\text{solv}}^*(T, P)]$  is its residual chemical potential at infinite dilution in the solvent (also referred to as its intrinsic hydration free energy,  $\Delta G_{\text{hyd}}(T, P)$ ), and the same quantity for the solvent is its self-solvation free energy; both are calculated by conventional MD simulations in the  $NVT$  ensemble.

The solvent chemical potential is obtained from the Gibbs–Duhem equation as<sup>porroozi2019efficient</sup>

$$\mu_{\text{solv}}(T, P; \mathbf{m}) = \mu_{\text{solv}}^\dagger(T; P) + RT \ln \left( \frac{1000}{M_{\text{solv}} m^0} \right) - RT \left( \frac{1 - x_{\text{solv}}}{x_{\text{solv}}} \right) \quad (4) \quad \text{eq:musolv}$$

We remark that for reactions in which the solvent (here water) participates, the solvent chemical potential is typically approximated in experimental studies by its Raoult Law form

$$\mu_{\text{solv}}(T, P; \mathbf{m}) = \mu_{\text{solv}}^*(T, P) + RT \ln(x_{\text{solv}}) \quad (5)$$



where  $\mu_{\text{solv}}^*(T, P)$  is the pure solvent chemical potential and  $x_{\text{solv}}$  is its mole fraction. Substitution of Eqs. (2)–(4) in Eq. (1) yields the final working equations:

$$\frac{\Delta\tilde{G}_j(T, P)}{RT} + \sum_{i=1}^{N_{\text{solv}}} \nu_{ij} \ln \left( \frac{m_i}{m^0} \right) + \nu_{\text{solv}} \left( -\frac{1 - x_{\text{solv}}}{x_{\text{solv}}} \right) = 0; \quad j = 1, 2, \dots, R \quad (6) \quad \text{eq: eqmcond}$$

where  $\nu_{\text{solv},j}$  is the stoichiometric coefficient of the solvent in reaction  $j$ , and

$$\Delta\tilde{G}_j(T, P) = \Delta G_j^0(T; P^0) + \Delta G_j^{\text{res}, NV T, \infty}(T, P) \quad (7)$$

$$+ RT \bar{\nu}_j \ln \left( \frac{RT M_{\text{solv}} m^0 \rho_{\text{solv}}^*(T, P)}{1000 P^0} \right) + \nu_{\text{solv},j} RT \ln \left( \frac{1000}{M_{\text{solv}} m^0} \right) \quad (8) \quad \text{eq: DeltaGd}$$

where

$$\Delta G_j^0(T; P^0) = \sum_{i=1}^{N_s} \nu_{ij} \mu_i^0(T; P^0) \quad (9) \quad \text{eq: IGcont}$$

$$\Delta G_j^{\text{res}, NV T, \infty}(T, P) = \sum_{i=1}^{N_s} \nu_{ij} \mu_i^{\text{res}, NV T, \infty}(T, P) \quad (10) \quad \text{eq: musim}$$

$$\bar{\nu}_j = \sum_{i=1}^{N_s} \nu_{ij} \quad (11)$$

$\Delta\tilde{G}_j(T, P)$  are commonly expressed in terms of equilibrium constants  $K_j$  via

$$pK_j(T, P) \equiv -\log_{10} K_j = \frac{\Delta\tilde{G}_j(T, P)}{RT \ln(10)} \quad (12) \quad \text{eq: pKdef}$$

We remark that the third term in Eq. 8 can be broken into a temperature dependent term, often referred to as “standard state correction” and density dependent term which often mistakenly ignored in the  $pK$  calculations ( see ref<sup>45</sup> for further details). <sup>poroozi2019prediction</sup>

### 3 Simulation Details

#### 3.1 Conformational Search and Ideal Gas Reaction Free Energies

To find the most stable conformer of the molecular/ionic species, an extensive gas phase conformational search of the geometry of the protonated, carbamate and neutral forms of each amine was performed using the Merck Molecular Mechanics Force Field (MMFF94) implemented in the Spartan v.18 Software package.<sup>[Spartan2018](#)</sup> For each species, using the 10 lowest energy conformers obtained from the MMFF94 search, we performed a further geometry optimization followed by frequency calculations using five different high-level composite quantum chemical (QM) methods: G4, G3, G3B3, CBS-QB3 and CBS-APNO in Gaussian16.<sup>[Gaussian09](#)</sup> We ensured that for each QM method, the conformer converged to a stable minimum of the potential energy surface with positive real vibrational frequencies. We then used the conformer with the lowest free energy/chemical potential for the subsequent ideal-gas reaction free energy calculation for each QM method.

#### 3.2 Force Field Development and Hydration Free Energy Calculations

All Lenard-Jones (LJ) and intramolecular bonded potential parameters of the solutes, including the bicarbonate ion ( $\text{HCO}_3^-$ ), the neutral amine ( $\text{RNH}_2$ ), and its protonated ( $\text{RNH}_3^+$ ) and carbamate ( $\text{RNHCO}_2^-$ ) form of the seven primary amines studied were modeled in a consistent manner using the General Amber Force Field<sup>[Wang2004](#)</sup> parameters within its default functional form. The atom type assignment was performed using the Antechamber package in AMBER tools,<sup>[Wang2006automatic](#)</sup> which uses a algorithm to determine the bonded parameters (bond, angle, and dihedral constants) based on the atom types. To calculate the partial charges, high-level QM methods are generally preferred to refine the geometry of the low-energy solute conformer. However, to be consistent with the ideal-gas geometry, we use the lowest free energy con-

former at the G4 level of the previous section as a representative of the solute gas-phase geometry. This was used to calculate its electrostatic potential energy grid at the HF/6-31G\* level using the Merz-Kollman scheme in Gaussian16. In addition to the GAFF default HF/6-31G\* level, we also examined the effects of partial charges determined from several different QM electron density determination methodologies (B3LYP/6-311++G(d,p), MP2 aug-cc pVTZ, and MP2 aug-cc pVTZ+PCM) on the resulting hydration free energies and equilibrium constants.

Finally, we used the two-step Restrained Electrostatic Surface Potential (RESP) fitting method<sup>[Bayly1993](#)</sup> within the Antechamber package to assign the partial charges. The Gromacs-formatted topologies were then generated using the acpype (version 2019) python interface.<sup>[da2012](#)</sup> Carbon dioxide (CO<sub>2</sub>) was modeled using the TraPPE potential of Pottoff,<sup>[Pottoff2001](#)</sup> and to be consistent with GAFF parametrization the solvent (water) was modeled with the TIP3P Force Field.

The MD simulations of the hydration free energies in Eq. [\(10\)](#)<sup>[eq:musim](#)</sup> were performed using a single solute molecule solvated in a periodic box of 1500 water molecules using the Gromacs (version 2016.3) program,<sup>[Pronk2013](#)</sup> with initial configurations generated using the packmol software package.<sup>[Martinez2009](#)</sup> A steepest-descent minimization was then performed to remove any bad contacts, followed by a short *NVT* equilibration run and a 12 ns *NPT* simulation to determine the system density. Free energy simulations to decouple the solute molecule from its solvent environment were then initiated from the equilibrated configurations in an *NVT* ensemble, with box size corresponding to the calculated density.

The equations of motion were integrated using the Gromacs stochastic Langevin scheme, with a friction constant of 1.0 ps<sup>-1</sup>. The pressure was maintained using a Parrinello-Rahman pressure coupling constant of 2.0 ps. The Lennard-Jones short-range interactions were smoothly switched off between 12 and 12.5 Å, and the electrostatic interactions were computed using the particle mesh Ewald (PME) method with a 12Å real-space cutoff, 1.0Å grid spacing, sixth-order spline interpolation, and accuracy of 10<sup>-6</sup>. The free energy of

a single solute molecule decoupling in the solvent environment was calculated using the Gromacs Bennett Acceptance Ratio (BAR) method (gmx bar). We employed six equally spaced  $\lambda$  values and linear decoupling for the electrostatic interaction, followed by 20 equally spaced  $\lambda$  values with  $\Delta\lambda = 0.05$  to decouple the LJ interactions using the standard GROMACS soft-core potential function originally proposed by Beutler et al.,<sup>Beutler1994</sup> with parameters (in GROMACS notation) *sc-alpha* = 0.5, *sc-power* = 1.0 and *sc-sigma* = 0.3. Each alchemical window was subjected to a 12.5 ns simulation with the first 2.5 ns discarded for equilibration.

## 4 Results and Discussion

### 4.1 Ideal-Gas Standard Reaction Free Energies

Tables S1 and S2 of the Supporting Information show our calculated ideal-gas standard reaction free energies  $\Delta G_j^0(T; P^0)$  for reactions (R1) and (R2) at four temperatures for the set of seven amines examined using five different composite QM methods. As noted by Somer et al.,<sup>Simmie2015benchmarking</sup> improved predictions can arise from the use of combinations of several-high level methods, since methods such as G4 tend to over-estimate and methods such as CBS-QB3 tend to underestimate the reaction free energy. The variations in the different method also enable us to infer the uncertainty rooted in the different chemical species of the same class of molecules. For example, in our previous work,<sup>poroozi2019prediction</sup> we found that for the amine species, the ideal gas free energies vary significantly among the QM methods, depending on the size and flexibility of the molecules involved. Based on the Table S1 results, for most species the Gaussian-n theories (G4, G3, G3B3) tend to predict higher  $\Delta G_j^0(T; P^0)$  values than those of the complete basis set (CBS-QB3, CBS-APNO) approaches. We note that the R2 values generally indicate slightly smaller standard deviations than those of R1, except for the species containing multiple hydroxyl groups (SAPD, AMPD, 2-AEE). For these species reaction R2 shows significant scatter among the QM methods.

For speciation calculations involving reactions (R1) and (R2), we used the average  $\Delta G_j^0(T; P^0)$  values from the five methods in Tables S1 and S2. Tables S8–S12 show the raw Gaussian16 output for each species from which they were calculated. Their standard deviations are about 3 kJ·mol<sup>-1</sup>, which we take as a surrogate measure of the uncertainty in the  $\Delta G_j^0(T; P^0)$  values. This value is well within a “chemical precision standard” of 1 kcal·mol<sup>-1</sup>.

## 4.2 $pK_1$ and $pK_2$ Results

Table 1 summarizes our  $pK_1$  and  $pK_2$  results for the seven alkanolamines studied at the indicated temperatures and  $P = 1$  bar. Their dependence on temperature is shown in Fig. 2, using regressions to the expression

$$pK = a + b/T + c \ln(T) \quad (13)$$

The values of the parameters ( $a, b, c$ ) are given in Table S3 of the SI.

The underlying data used for the  $pK$  calculations is given in the Supplementary Information as follows. Table S4 shows the simulated  $\mu^{\text{res}, NV T, \infty}(T, P)$  values for the neutral (RNH<sub>2</sub>), protonated (RNH<sub>3</sub><sup>+</sup>) and carbamate (RNHCO<sub>2</sub><sup>-</sup>) forms of the seven alkanolamines at the four temperatures of this study. Table S5 shows  $\mu^{\text{res}, NV T, \infty}(T, P)$  values for HCO<sub>3</sub><sup>-</sup>, for CO<sub>2</sub> using the Trappe FF,<sup>Potoff2001</sup> and for H<sub>2</sub>O using the TIP3P FF. The  $\Delta \tilde{G}_j(T, P)$  and  $pK_j(T, P)$  values for reactions (R1) and (R2) used in the reaction equilibrium calculations listed in Tables S6 and S7.

The indicated uncertainties in Table 1 are one standard deviation, which are seen to be within a “chemical precision standard” of 1 kcal·mol<sup>-1</sup> for  $\Delta \tilde{G}_j(T, P)$  in Eq. (8). This translates to a precision in  $pK$  units of

$$\Delta pK = \frac{4184}{2.303RT} = \frac{218.506}{T} \quad (14)$$

which at 298.15 K is 0.73  $pK$  units. Interestingly, as shown in Fig. 2, compared to car-

bamate forming amines, for the sterically hindered amines one can see a weak temperature dependence of the equilibrium constant of carbamate reversion reaction.

Table 1: Predicted  $pK$  values for reactions (R1) and (R2) from this work at the indicated temperatures and  $P = 1$  bar.

$T$ (K)	MEA	AMP	1-AP	AMPD	SAPD	2-AEE	2-AP
Reaction (R1)							
298.15	-5.75 <sub>0.56</sub>	-2.29 <sub>0.58</sub>	-3.89 <sub>0.66</sub>	-2.24 <sub>0.52</sub>	-3.63 <sub>0.62</sub>	-5.84 <sub>0.50</sub>	-3.57 <sub>0.49</sub>
313.15	-4.84 <sub>0.54</sub>	-1.58 <sub>0.55</sub>	-3.08 <sub>0.63</sub>	-1.69 <sub>0.51</sub>	-2.95 <sub>0.59</sub>	-4.93 <sub>0.49</sub>	-2.88 <sub>0.46</sub>
333.15	-3.83 <sub>0.49</sub>	-0.74 <sub>0.52</sub>	-2.30 <sub>0.60</sub>	-0.80 <sub>0.50</sub>	-2.11 <sub>0.55</sub>	-3.77 <sub>0.48</sub>	-2.05 <sub>0.44</sub>
353.15	-3.20 <sub>0.50</sub>	-0.01 <sub>0.49</sub>	-1.61 <sub>0.58</sub>	-0.32 <sub>0.49</sub>	-2.05 <sub>0.51</sub>	-2.63 <sub>0.48</sub>	-1.37 <sub>0.41</sub>
Reaction (R2)							
298.15	1.62 <sub>0.42</sub>	-1.87 <sub>0.50</sub>	0.61 <sub>0.40</sub>	-1.02 <sub>0.60</sub>	-0.095 <sub>0.53</sub>	1.22 <sub>0.66</sub>	-0.26 <sub>0.48</sub>
313.15	1.38 <sub>0.40</sub>	-1.93 <sub>0.49</sub>	0.43 <sub>0.39</sub>	-1.08 <sub>0.59</sub>	-0.19 <sub>0.51</sub>	0.90 <sub>0.65</sub>	-0.34 <sub>0.47</sub>
333.15	1.15 <sub>0.39</sub>	-1.90 <sub>0.47</sub>	0.30 <sub>0.37</sub>	-1.16 <sub>0.57</sub>	-0.28 <sub>0.49</sub>	0.59 <sub>0.63</sub>	-0.42 <sub>0.45</sub>
353.15	1.15 <sub>0.38</sub>	-1.90 <sub>0.46</sub>	0.25 <sub>0.36</sub>	-1.14 <sub>0.55</sub>	-0.38 <sub>0.48</sub>	0.18 <sub>0.62</sub>	-0.47 <sub>0.44</sub>

table:pKresults

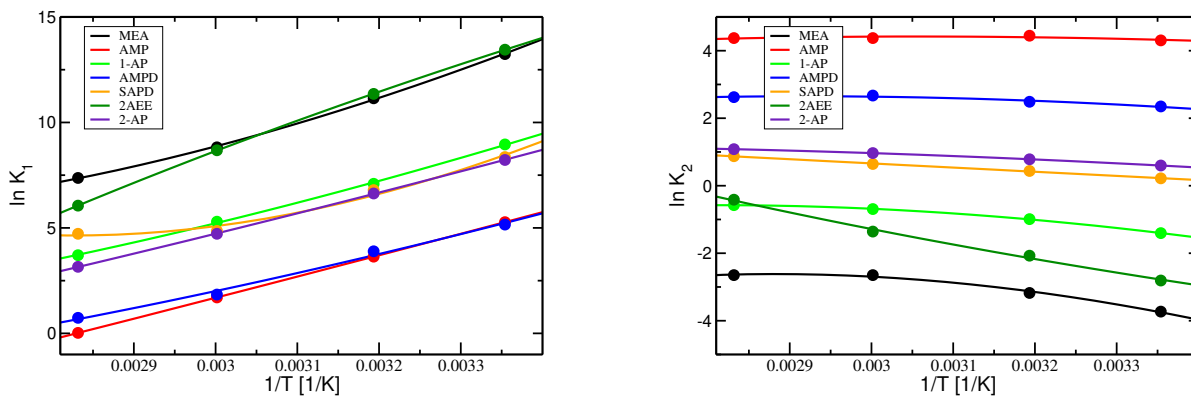


Figure 2: Temperature dependence of the equilibrium constants for reactions (R1) and (R2) for the seven amines studied.

g:pKvalues

### 4.3 Impact of Different Partial Charge Methods on the $pK$ Values

As described in Section [3](#),<sup>[sec:simdetails](#)</sup> for the  $pK$  calculations and the resulting equilibrium compositions we used GAFF default HF/6-31G\* partial charges based on each molecule’s G4 optimized geometry, from which the electrostatic surface grid and the RESP atomic partial charges were obtained. Numerous studies<sup>[mobley2007comparison](#), [jambeck2013partial](#)</sup> have addressed the effects on the  $\mu^{\text{res}, NV T, \infty}$  values of different QM approaches used to obtain the FF partial charges. To examine this effect for our systems, we considered representative  $\mu^{\text{res}, NV T, \infty}$  values for MEA and for AMP at  $T = 298.15$  K based on RESP partial charge assignment arising from several different QM methodologies: the default GAFF HF/6-31G\* results from Table S3, B3LYP/6-311++G(d,p), MP2/agu-cc-pVTZ) in the gas phase and a MP2/agu-cc-pVTZ calculation in presence of polarizable continuum solvent (MP2/agu-cc-pVTZ+PCM, with a dielectric constant of 78.39). These are shown in Table [2](#).<sup>[table:AMP-MEA-FE](#)</sup>

Table 2: Comparison of GAFF predicted intrinsic hydration free energies,  $\mu^{\text{res}, NV T, \infty}$  (in  $\text{kJ} \cdot \text{mol}^{-1}$ ) of the protonated, neutral and carbamate forms of MEA and AMP at  $T = 298.15$  K using different sets of partial charges in conjunction with RESP.

AMP-MEA-FE

Species	MP2/aug-cc-pVTZ+PCM	HF/6-31G*	B3LYP/6-311G**	MP2/agu-cc-pVTZ
monoethanolamine (MEA)				
RNH <sub>2</sub>	-32.89 <sub>0.05</sub>	-30.23 <sub>0.14</sub>	-26.94 <sub>0.19</sub>	-23.30 <sub>0.07</sub>
RNH <sub>3</sub> <sup>+</sup>	-243.87 <sub>0.09</sub>	-239.43 <sub>0.10</sub>	-235.95 <sub>0.1</sub>	-234.71 <sub>0.13</sub>
RNHCOO <sup>-</sup>	-400.63 <sub>0.08</sub>	-366.79 <sub>0.19</sub>	-365.63 <sub>0.15</sub>	-358.62 <sub>0.27</sub>
2-amino-2-methylpropanol (AMP)				
RNH <sub>2</sub>	-38.53 <sub>0.03</sub>	-34.35 <sub>0.13</sub>	-31.68 <sub>0.16</sub>	-27.50 <sub>0.07</sub>
RNH <sub>3</sub> <sup>+</sup>	-228.33 <sub>0.06</sub>	-222.50 <sub>0.11</sub>	-216.22 <sub>0.13</sub>	-215.57 <sub>0.12</sub>
RNHCOO <sup>-</sup>	-393.84 <sub>0.06</sub>	-352.33 <sub>0.10</sub>	-349.64 <sub>0.12</sub>	-342.94 <sub>0.04</sub>

The results show relatively small (3–8  $\text{kJ} \cdot \text{mol}^{-1}$ ) differences from our default HF/6-31G\* calculations in the cases of B3LYP/6-311G\*\* and MP2/agu-cc-pVTZ). However, when the polarizable continuum model (PCM) is included in the calculation of the electron density (MP2-aug-cc-pVTZ+PCM), the hydration free energy of the CO<sub>2</sub>-bound anion (RNHCO<sub>2</sub><sup>-</sup>) becomes too negative (by more than 40 kJ) compared to the unpolarized charges (mp2-aug-cc-pVTZ) result. In contrast, the change derived from the polarized electronic density affects

the hydration free energy of the protonated amines ( $\text{RNH}_3^+$ ) to a lesser extent (around 10 kJ). Partial charges obtained from the RESP methodology already tend to over polarize anions in the absence of PCM,<sup>Kroutil2017</sup> and our results show that this becomes excessive in its presence.

Representative  $pK$  values at 298.15 K for reactions (R1) and (R2) calculated from Eqs (8)–(12) using columns 3–5 of Table 2 and the data of Tables S1, S2 and S4 are shown in Table 3. Whereas the  $\mu^{\text{res}, NV T, \infty}$  vary substantially across the QM levels in Table 2, the  $pK$  values in Table 3 are not overly sensitive to the different partial charge methodologies.

Table 3: Comparison of the predicted  $pK$  values of reactions (R1) and (R2) for the MEA and AMP systems at  $T = 298.15$  K using different sets of partial charges from Table 2, the  $\Delta G^0$  values in Table S1 and S2, and the  $\mu^{\text{res}, NV T, \infty}$  values for  $\text{H}_2\text{O}$ ,  $\text{CO}_2$  and  $\text{HCO}_3^-$  in Table S4.

Reaction	HF/6-31G*	B3LYP/6-311G**	MP2/agu-cc-pVTZ
monoethanolamine (MEA)			
R1	-5.75 <sub>0.56</sub>	-6.09 <sub>0.56</sub>	-5.92 <sub>0.56</sub>
R2	1.62 <sub>0.42</sub>	2.00 <sub>0.41</sub>	1.41 <sub>0.41</sub>
2-amino-2-methylpropanol (AMP)			
R1	-2.29 <sub>0.58</sub>	-1.64 <sub>0.58</sub>	-1.81 <sub>0.58</sub>
R2	-1.87 <sub>0.50</sub>	-1.85 <sub>0.50</sub>	-1.31 <sub>0.50</sub>

## 4.4 Carbamate Formation/Stability Constant, $K_2$

In this section we discuss our  $K_2$  results in comparison with those obtained from experiment at 298.15 K when such data is available.

In our approach, we directly predict the equilibrium constant  $K_2(T, P)$  for the carbamate reversion reaction (R2) from simulation quantities using Eq. (12).  $K_2(T, P)$  cannot be directly measured experimentally, but must be obtained indirectly using either of the equations

$$K_2(T, P) = \prod_{i=1 \dots N_s} [m_i^* \gamma_i(T, P; \mathbf{m}^*)]^{\nu_{i2}} \quad (15) \quad \text{eq:K\_exp}$$



$$\ln K_2(T, P) = \sum_{i=1}^{N_s} [\nu_{i2} [\ln m_i^* + \ln \gamma_i(T, P; \mathbf{m}^*)]] \quad (16) \quad \boxed{\text{eq:K\_exp2}}$$

where the molalities and activity coefficients refer to an experimentally measured equilibrium composition,  $\mathbf{m}^*$ , and  $\nu_{i2}$  is the reaction stoichiometric coefficient of species  $i$  in reaction (R2). One approach is by means of extrapolation to zero ionic strength of the experimentally measured species activity coefficient ratio of Eq. (I5), and another is to fit the measured equilibrium data to the calculated equilibrium composition from a thermodynamic model for the activity coefficients as a function of composition using Eq. (I6).

Our predicted  $pK_2$  values at the representative temperature  $T = 298.15$  K are shown in Table 4, where they are compared with experimental results from the literature. The major source of uncertainty in our  $pK$  calculations is that of the ideal-gas  $\Delta G_2^0$  term in Eq (9). For the experimental values, the sources of uncertainty/error in  $pK_2$  are the uncertainties in any model used for the activity coefficients and the uncertainties in the experimental composition measurements. The latter is likely the greater contributor, since both the neutral amine and its protonated form are involved in the carbamate reversion reaction, and it is very difficult to experimentally distinguish the forms from NMR data and to thereby establish the individual concentrations of each form.

We have already noted that our  $pK$  uncertainties are within a “chemical precision standard” of 0.73  $pK$  units at 298.15 K. We remark that the precisions of experimental studies are often not provided, but we highlight the careful experimental work of the Tremaine group,<sup>McGregor2018</sup> which recently studied  $pK_2$  values from 283.2–313.2 K for 2-methylpiperadine using NMR spectroscopy and reported precisions using of 0.35–1.50  $pK$  units. ••• is this  $pK$  unit? •••.

Table 4: Comparison with literature data of calculated  $pK_2$  for the carbamate reversion reaction (eq:R2) at  $T = 298.15$  K (unless indicated otherwise) and  $P = 1$  bar .

Amine	This work, Table 2	Literature
monoethanolamine(MEA)	1.62 <sub>0.42</sub>	1.71(291.15 K) <sup>17,18,69,72,75</sup> 1.25 <sup>68</sup> 1.31 <sup>69</sup> 1.81 <sup>70</sup> 1.46 <sup>71</sup> 1.60 <sup>72</sup> 1.76 <sup>69,73</sup> <sup>conway2013toward</sup>
2-amino-2-methyl-1-propanol(AMP)	-1.87 <sub>0.50</sub>	-0.47 <sup>73</sup> <sup>conway2013toward</sup>
1-amino-2-propanol(1-AP)	0.61 <sub>0.40</sub>	1.70 <sub>0.2</sub> <sup>75</sup>
2-amino-2-methyl-1,3-propanediol(AMPD)	-1.02 <sub>0.60</sub>	sterically hindered <sup>76</sup>
2-(2-aminoethoxy)ethanol(2-AEE)	1.22 <sub>0.66</sub>	1.75 <sup>76</sup>
serinol(2-aminopropane-1,3-diol)(SAPD)	-0.09 <sub>0.53</sub>	no carbamate detected <sup>75</sup>
2-amino-1-propanol(2-AP)	-0.26 <sub>0.48</sub>	-0.6 <sub>0.1</sub> , <sup>75</sup> 0.98 <sup>18</sup>

table:IG

$pK_2(T, P)$  for MEA has been the subject of numerous experimental studies, <sup>17,18,69,72,75</sup> around 1999 equilibrium, mcca using the indicated approaches or variants thereof. For MEA at 298.15 K, our predictive methodology gives  $pK_2 = 1.62 \pm 0.42$ . The spread of the literature  $pK$  values (1.25–1.81) is partly due to differences in the activity coefficient models used by the authors, and likely more importantly to the difficulty in the measurement of the concentrations of the proton exchanging species. The precision of our calculations is seen to be similar to that of the experimental data.

There are fewer experimental  $pK$  results for the other alkanolamines. Our predicted AMP value is  $pK_2 = -1.87 \pm -0.50$ . McCann *et al.* <sup>mccann2011systematic</sup> studied carbamate formation in the AMP system using  $^1\text{H}$  NMR. They did not detect carbamate, but they noted that  $pK_2 < -0.70$  at 303 K. Sartori and Savage <sup>sartori1983sterically</sup> reported an “apparent equilibrium constant” for AMP in their  $^{13}\text{C}$  NMR study of  $pK_2 < -1.0$  at 313 K. This approximation assumes that the AMP activity coefficients for  $\text{RNHCO}_2^-$  and  $\text{HCO}_3^-$  are equal at finite concentrations and hence cancel in the activity coefficient ratio. This behaviour is inferred from the fact that this holds exactly in the Debye–Hückel activity coefficient model, which predicts activity coefficients for ions that depend only on their charge, and the iso–Coulombic reaction (eq:R2) leads to the cancellation at finite concentrations. We can see supporting evidence for this approximation from the  $\mu^{\text{res}, NV T, \infty}$  values for  $\text{RNHCO}_2^-$  and  $\text{HCO}_3^-$  in Tables S3 and S4 of the Supporting

Information, where it is seen that the quantities are of the same sign and similar magnitude. We also found (not shown) that simulations show that the corresponding difference remains roughly constant as the concentrations are increased. Using the same assumption, Yamada *et al.* reported  $pK_2 \approx -1.0$  for AMP from  $^{13}\text{C}$  NMR studies at 298.15K. The negative AMP  $pK_2$  value compared to that of MEA indicates that AMP carbamate formation is thermodynamically less favoured, a consequence of the steric effect of the two methyl groups ( $-\text{CH}_3$ ) on the  $\alpha$  carbon connected to the amine nitrogen atom. Evidence of the experimental difficulty of observing carbamate is shown in Fig. 3 in Section 4.6, where it is seen that the AMP carbamate concentration is less than  $10^{-4}$ .

Removing one of the  $-\text{CH}_3$  groups from the  $\alpha$  carbon of AMP gives 2-AP. For 2-AP, the predicted  $pK_2$  value increases to  $pK_2 = -0.26 \pm 0.48$ , which lies between that of MEA and AMP. Fernandes *et al.*<sup>16</sup> reported a value of  $pK_2 = 0.98$  at 298.15 K for 2-AP from their NMR study, which is significantly higher than our value. In a more recent study by the same group,<sup>15</sup> they obtained  $pK_2 = -0.60 \pm 0.1$ , which agrees with our predicted value within their mutual uncertainties, indicating that the molecular models employed here are able to predict the trend in steric effects.

The addition of a ( $-\text{CH}_3$ ) to the  $\beta$  carbon of MEA gives 1-AP. For this molecule, we predict a carbamate formation constant of  $pK_2 = 0.61 \pm 0.40$  which is smaller than that of MEA. This indicates little steric effect from the  $-\text{CH}_3$  group further away from the amino group. While the experimental study also noted significant carbamate formation in the 1-AP solution, the equilibrium constant for 1-AP reported by Conway *et al.* is  $pK_2 = -1.7$ . For 2-AEE, we predicted a  $pK_2 = 1.21 \pm 0.66$  at 298.15 K and this system was experimentally studied by Al-Juaied *et al.*<sup>16</sup> using  $^{13}\text{C}$  NMR. They reported an apparent  $pK_2 = 1.75$  for 17.7 M DGA at relatively low  $\text{CO}_2$  loading at 300 K. (See the iso-Coulombic discussion above.) While Conway *et al.*<sup>15</sup> did not observe carbamate formation in SAPD, Bougie *et al.*<sup>18</sup> suggested carbamate formation in SAPD similar to unhindered amines based on the trend of solubility data. For SAPD, we predicted a value of  $pK_2 = -0.09 \pm 0.53$

at 298.15 K indicating that it is a mild carbamate forming amine. We did not find any experimental data of carbamate/bicarbonate for AMPD, and similar to AMP, it is a sterically hindered amine and our predicted value of AMPD carbamate formation constant found to be  $pK_2 = -1.02 \pm 0.60$ . Generally, comparison with the limited experimental data shows that the molecular models employed here are able to capture qualitative and to a reasonable accuracy a quantitative trend in carbamate formation of the common primary and secondary amines used in the PCC process.

## 4.5 Consistency Tests for the Amine Protonation Constants

For a wide range of amines, experimental  $pK$  data are available for the amine protonation reaction (R8)<sup>[eq:R8](#)</sup><sup>[Duffy2009](#)</sup> and the equilibrium constants for Reactions R3, R4 and R5 are well studied, based on the  $\text{CO}_2 - \text{H}_2\text{O}$  equilibria for a wide range of temperatures.<sup>[edwards1978vapor](#)</sup> Since Reaction (R8) is the sum ([eq:R1](#))+(R2)-(R3), this allows the prediction of any one of the equilibrium constants from those of the others. In Table [table:pk8predict](#) 5, we show predictions of  $pK_8$  from our simulation results for the equilibrium constants of reactions ([eq:R1](#)), ([eq:R2](#)), and the experimental data of Edwards *et al.*<sup>[edwards1978vapor](#)</sup> for the bicarbonate reaction ([eq:R3](#)). This approach allows the prediction of amine protonation  $pK_8$  values that are independent of knowledge of the absolute hydration free energy of the proton,  $\Delta G^{Hydr}(H^+)$ , a precise value of which remains unknown despite extensive experimental and theoretical efforts. It is seen that the  $pK_8$  values predicted in this way are generally within 1  $pK$  unit of the experimental values. Since  $pK_2$  agrees well with the experimental values and the only species not appearing in both ([eq:R1](#)) and ([eq:R2](#)) is the protonated amine species,  $\text{RNH}_3^+$ , we suggest that an improved treatment of this species would lead to better agreement with the experimental  $pK_8$  values.

Table 5: Prediction of the amine protonation constant ( $pK_8$ ) independently of knowledge of the proton ( $H^+$ ) hydration free energy at 298.15 K using  $pK_8 = pK_1 + pK_2 - pK_3$ , in conjunction with our results for  $pK_1$  and  $pK_2$  in Table I and the well-established experimental value  $pK_3 = 6.30^{80}$  for the bicarbonate reaction.

amine	$-pK_8$ (this work)	$-pK_8$ (expt)
MEA	10.42 <sub>0.50</sub>	9.51 <sub>0.81</sub> <sup>Liu2019</sup> , 9.44 <sub>0.82</sub> <sup>Hamborg2009</sup> , 9.50 <sub>0.84</sub> <sup>Patel1951</sup> , 9.51 <sub>0.84</sub> <sup>Kim1987</sup> 9.59 <sub>0.19</sub> <sup>Antelo1988</sup> , 9.50 <sub>0.86</sub> <sup>Antelo1988</sup> , 9.44 <sub>0.87</sub> <sup>Antelo1988</sup>
AMP	10.45 <sub>0.52</sub>	9.67 <sub>0.01</sub> <sup>fernandes2012investigations</sup>
1-AP	9.57 <sub>0.56</sub>	9.50 <sub>0.18</sub> <sup>fernandes2012investigations</sup>
AMPD	9.63 <sub>0.44</sub>	8.84 <sub>0.01</sub> <sup>fernandes2012investigations</sup>
SAPD	10.07 <sub>0.55</sub>	8.55 <sub>0.18</sub> <sup>fernandes2012investigations</sup>
2-AEE	10.97 <sub>0.48</sub>	9.42 <sub>0.18</sub> <sup>fernandes2012investigations</sup>
2-AP	10.13 <sub>0.52</sub>	9.52 <sub>0.01</sub> <sup>fernandes2012investigations</sup> , 9.40 <sub>0.18</sub> <sup>fernandes2012investigations</sup>

table: pK <sub>a</sub> of dipK
--------------------------------

## 4.6 Speciation Predictions

Whereas there exists extensive CO<sub>2</sub> solubility data as a function of its partial pressure for a wide range of amines, only a few NMR-based studies have dealt with speciation data in the solvent.<sup>bottinger2008online, ciftja2014experimental, jakobsen2005liquid, Hilliard2008</sup> For the amines considered in this work, we only found NMR measurements for MEA and for AMP, which are shown in Fig. 3. Fig. 3 shows our predicted species distributions in MEA and in AMP as a function of CO<sub>2</sub> loading using the Henry-law based chemical potential model, in comparison with available experimental data. The top panel indicates the speciation using only reactions <sup>eq:R1</sup>R1 and <sup>eq:R2</sup>R2, ignoring the the minor species {CO<sub>3</sub><sup>-2</sup>, H<sup>+</sup>, OH<sup>-</sup>} and the bottom panel shows the same calculation using all nine species in the calculation employing well established experimental value for the equilibrium constant of the CO<sub>2</sub>-water system (reaction <sup>eq:R3</sup>R3, <sup>eq:R4</sup>R4 and <sup>eq:R5</sup>R5)<sup>edwards1978vapor</sup> along with our predicted values for the <sup>eq:R1</sup>R1 and <sup>eq:R2</sup>R2. In the case of MEA, inclusion of these species only slightly affects the HCO<sub>3</sub><sup>-</sup> concentration at low loading, and the major species concentrations are unaffected. For AMP, the inclusion of the CO<sub>3</sub><sup>-2</sup> ion in the speciation calculations slightly lowers the HCO<sub>3</sub><sup>-</sup> and AMPCO<sub>3</sub><sup>-</sup> concentrations. Overall, it is a good approximation to ignore reactions R3–R5 in

the equilibrium calculations. In Fig. [fig:speciation\\_MEA\\_AMP](#), the filled circles are experimental data from the Bottinger *et al.*<sup>[bottinger2008](#)</sup> or Hillard<sup>[hillard2008](#)</sup>. Our result for species (MEA/MEA<sup>+</sup>, HCO<sub>3</sub><sup>-</sup>/CO<sub>3</sub><sup>-2</sup> pairs and MEACO<sub>2</sub><sup>-</sup>) distribution is in reasonable agreement with the NMR data. The open circles are the data from Jakobson *et al.*<sup>[jakobsen2005liquid](#)</sup>. The concentration of the HCO<sub>3</sub><sup>-</sup>/CO<sub>3</sub><sup>-2</sup> pair reported by Jakobson is in reasonable agreement with that of ours, whereas Hillard data (filled blue circles) seems to underpredict HCO<sub>3</sub><sup>-</sup>/CO<sub>3</sub><sup>-2</sup> concentration at low loading region. The isolated HCO<sub>3</sub><sup>-</sup> concentration of Jakobson agrees well with ours, but CO<sub>3</sub><sup>-2</sup> concentration is significantly higher at higher loadings. Jakobson used a thermodynamics model to separate the concentration of HCO<sub>3</sub><sup>-</sup>/CO<sub>3</sub><sup>-2</sup> pairs obtained from NMR. We remark that Jakobson data does not obey electro-neutrality, which they contributed to a possible overestimation of CO<sub>3</sub><sup>-2</sup> ions concentration. At low CO<sub>2</sub> loading where species are present in minor concentrations, it is extremely difficult to experimentally detect such species concentrations, and there are significant scatter in the reported species concentration. This also results in significant uncertainty in the “equilibrium constant” of the carbamate formation reaction (often called the carbamate stability constant) reported in the literature based on NMR data. The MEACO<sub>2</sub><sup>-</sup> concentration of Jakobsen (green open circles) also is significantly higher than that of Bottinger, who used a combination of <sup>13</sup>C and <sup>1</sup>H NMR with the goal of obtaining more accurate carbamate concentration.

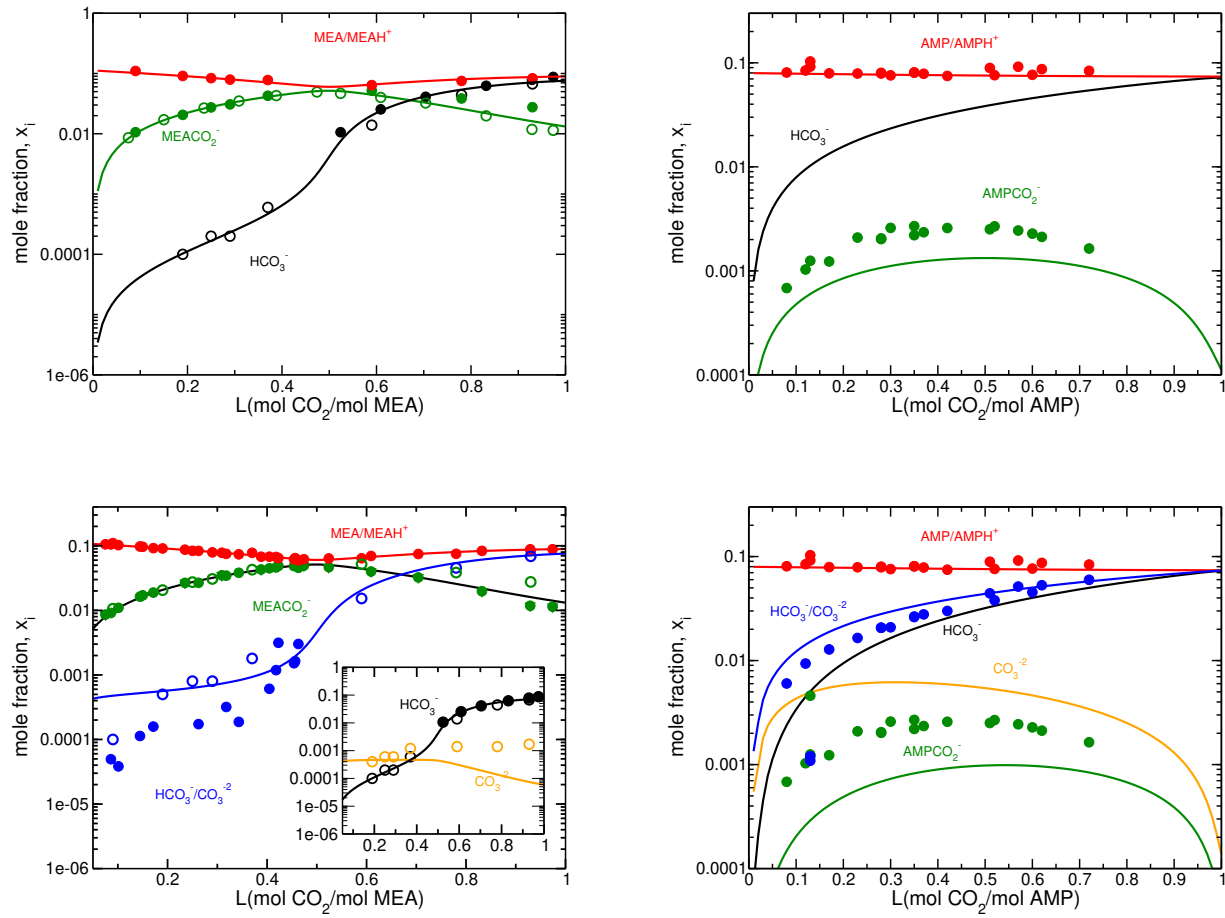


Figure 3: Speciation predictions (curves) for 30 wt% aqueous MEA and AMP solutions of  $\text{CO}_2$  at  $T = 298.15 \text{ K}$  and  $P = 1 \text{ bar}$ , and their comparison with experimental data. The top panel shows our results obtained by considering only reactions R1 and R2 and the bottom panel includes all species. Curves show the predicted results and symbols indicate experimental data. Different colors indicate different species. For MEA, open circles denote data of Jakobsen *et al.*,<sup>68</sup> filled circles denote data of Hilliard<sup>89</sup> and Bottinger.<sup>70</sup> Experimental data for AMP are from Ciftja *et al.*<sup>73</sup>

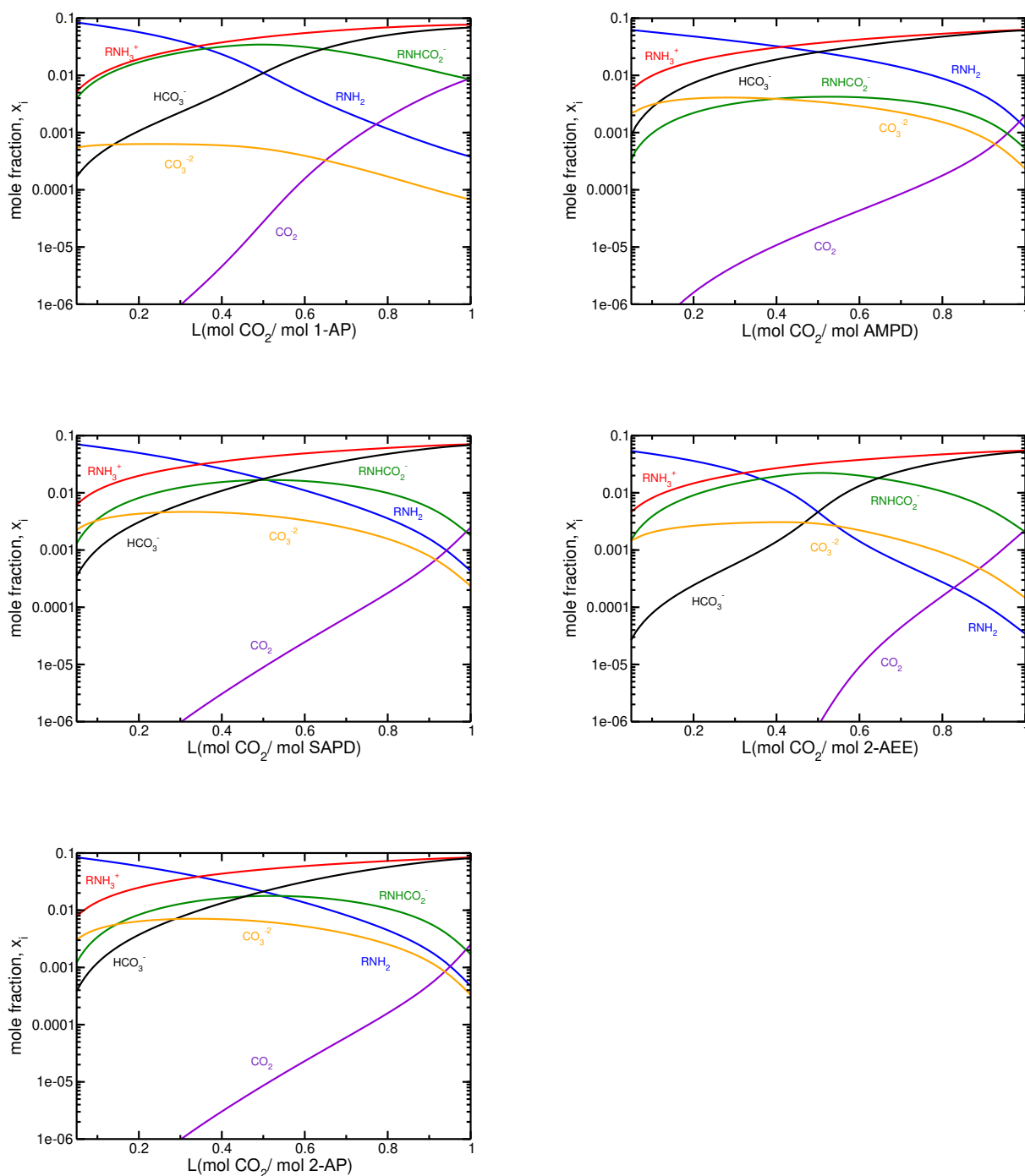


Figure 4: Speciation predictions (curves) for reactive absorption of  $\text{CO}_2$  in 30 wt% amine aqueous solutions at  $T = 298.15 \text{ K}$  and  $P = 1 \text{ bar}$ . No experimental data exists for comparison.

In contrast to MEA, which is a carbamate forming species, AMP is a sterically hindered



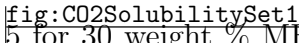
amine and forms only very small amounts of carbamate, due to the electronic effect of the methyl groups around the nitrogen. As shown in Fig3 <sup>fig:speciation\_MEA\_AMP</sup> this is well captured in our simulation predictions. Our predicted concentration of  $\text{HCO}_3^-/\text{CO}_3^{2-}$  pair is in good agreement with the Ciftja *et al.* measurements, while the the  $\text{AMPCO}_2^-$  concentration is significantly higher. The disagreement of  $\text{AMPCO}_2^-$  concentration with the experimental NMR-based data of Ciftja *et al.* <sup>ciftja2014experimental</sup> can be justified due to the fact that the speciation fraction data reported by Ciftja *et al.* does not obey electroneutrality, resulting in the likelihood that the carbamate concentrations are subject to significant uncertainties.

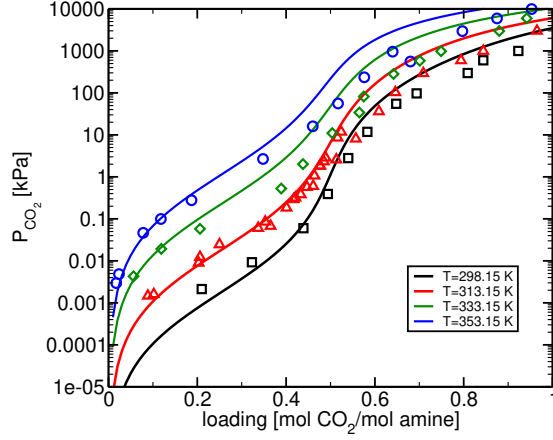
We remark that the predicted speciation curves are very sensitive to the reaction equilibrium constant only for the species with minor concentration. At low loadings, the amount of physically dissolved  $\text{CO}_2$  is extremely sensitive to the  $pK_a$  of the main reaction (<sup>eq:R1</sup>R1) while the amount of bicarbonate ion is sensitive to the equilibrium constant of the carbamate reversion reactions (<sup>eq:R2</sup>R2) and reasobale agreement of these species concentration with the experimental values indicate the accuracy of the predicted equilibrium constants for these two reactions and these parameters vary significantly from differences of only a few kJ in the hydration free energies due to exponential dependency of the reaction equilibrium constant on the reaction free energy.

## 4.7 $\text{CO}_2$ Solubility

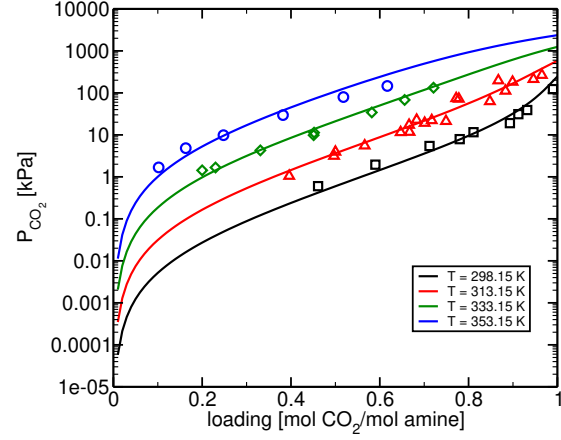
The equilibrium solubility of  $\text{CO}_2$  expressed in terms of the partial pressure of  $\text{CO}_2$  in the vapour phase as function of the total (both physically dissolved and chemically bound)  $\text{CO}_2$  loading in solution phase. It is determined from the equality of its solution and vapour phase chemical potentials. At the relatively low total pressure, the vapour phase may be treated as an ideal gas, which yields the following equation for the  $P_{\text{CO}_2}$

$$\tilde{P}_{\text{CO}_2} = \left( \frac{RT}{100P^0} \right) \left( \frac{\bar{\rho}_{\text{solv}}(T, \tilde{P})}{1000} \right) m_{\text{CO}_2} \exp \left( \frac{\mu_{\text{CO}_2}^{\text{res}, NV T, \infty}(T, \rho(T, \tilde{P}))}{RT} \right) \quad (17) \quad \text{eq:PC02fin}$$

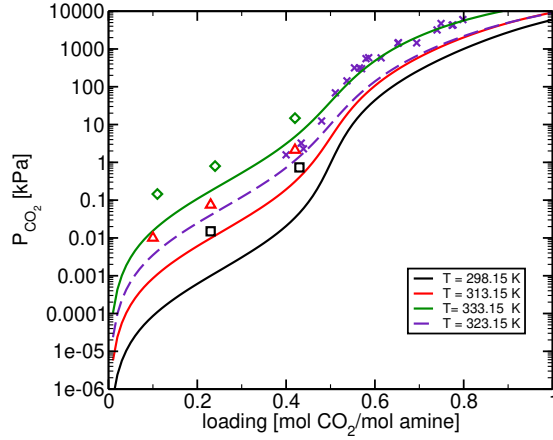
We ignore the small pressure dependence of the simulation quantities in this expression, and use our simulated values calculated at  $P = 1$  bar. The above equation is based on an ideal solution chemical potential model and ignores the slight composition dependency of the  $\text{CO}_2$  residual chemical potential. The dependence of  $P_{\text{CO}_2}$  on loading at the temperatures considered is shown in Fig.  5 for 30 weight % MEA, AMP, AMPD and 60 weight % 2-(2-aminoethoxy)ethanol (2-AEE) or diglycolamine (DGA). We note that for aqueous 2-AEE system, at limit of zero loading, the mole fraction of amine would be around  $x \approx 0.18$  and assumption of Henry law ideal solution may not hold and we did not find any data for low weight fraction. Generally, the predicted  $P_{\text{CO}_2}$  data are in reasonable agreement with the available experimental data over the temperature range considered. We note that,  $P_{\text{CO}_2}$  is extremely sensitive to the equilibrium constant of the reactions and the agreement with the experiment is very promising and suggesting that the reaction equilibrium constants can be predicted with reasonable accuracy.



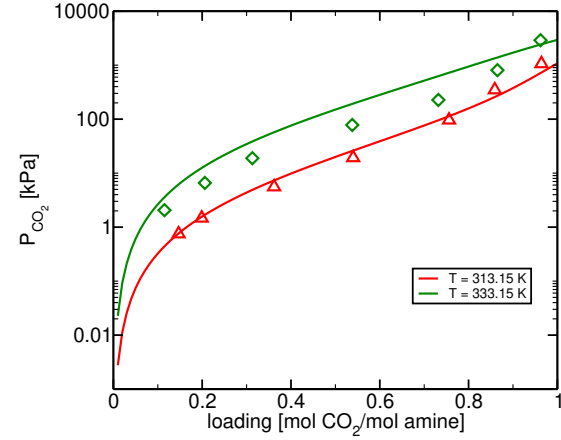
a) MEA



b) AMP



c) 2-AEE



d) AMPD

Figure 5: Comparison of the CO<sub>2</sub> partial pressures in 30 weight% MEA, AMP, AMPD and 60% 2-AEE aqueous solutions using the Henry-law-based ideal-solution model at different temperatures with experimental data. In the case of 2-AEE, stars indicate the experimental data of Martin *et al.* and the other symbols are data of Al-Juaied *et al.* (65 wt% 2-AEE).

For the 2-AP system, we only found a single solubility measurement at 313.15 K, with a CO<sub>2</sub> partial pressure of 15 kPa over 2M (16 wt %) 2-AP aqueous solution agreeing well with our predicted value shown in Fig.6.

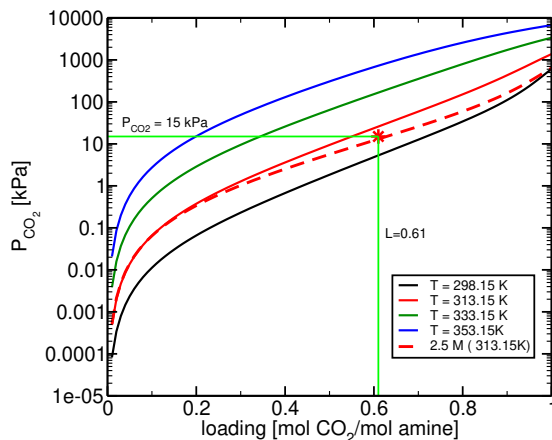


Figure 6: CO<sub>2</sub> solubility in 30 wt% (solid lines) and 16 wt% (dashed red line) 2-AP .

## 5 Effect of Amine Concentration on CO<sub>2</sub> Solubility

Optimizing the amine concentration in the solvent is an important parameter for PCC system design. Our equilibrium model can be used to evaluate the effect of the amine concentration on gas solubility without any additional data. It can be seen that for the carbamate forming amines (MEA, 1-AP, SAPD) amine concentration has little effect on the CO<sub>2</sub> solubility for loading range below  $\alpha \approx 0.5$ . At loading range  $\alpha \geq 0.5$ , less amine-concentrated solution will have a better CO<sub>2</sub> solubility. This is contributed to the change in reaction mechanism from carbamate formation to bicarbonate formation. This “salting out” effect is more pronounced for the MEA which is an strong carbamate forming species, while less pronounced for SAPD which we found to be a mild carbamate forming molecule. Similar to the MEA, 1-AP is a carbamate forming solvent and amine concentration is expected to have little effect on CO<sub>2</sub> solubility at low loading, while the experimental data looks scattered at low loading.

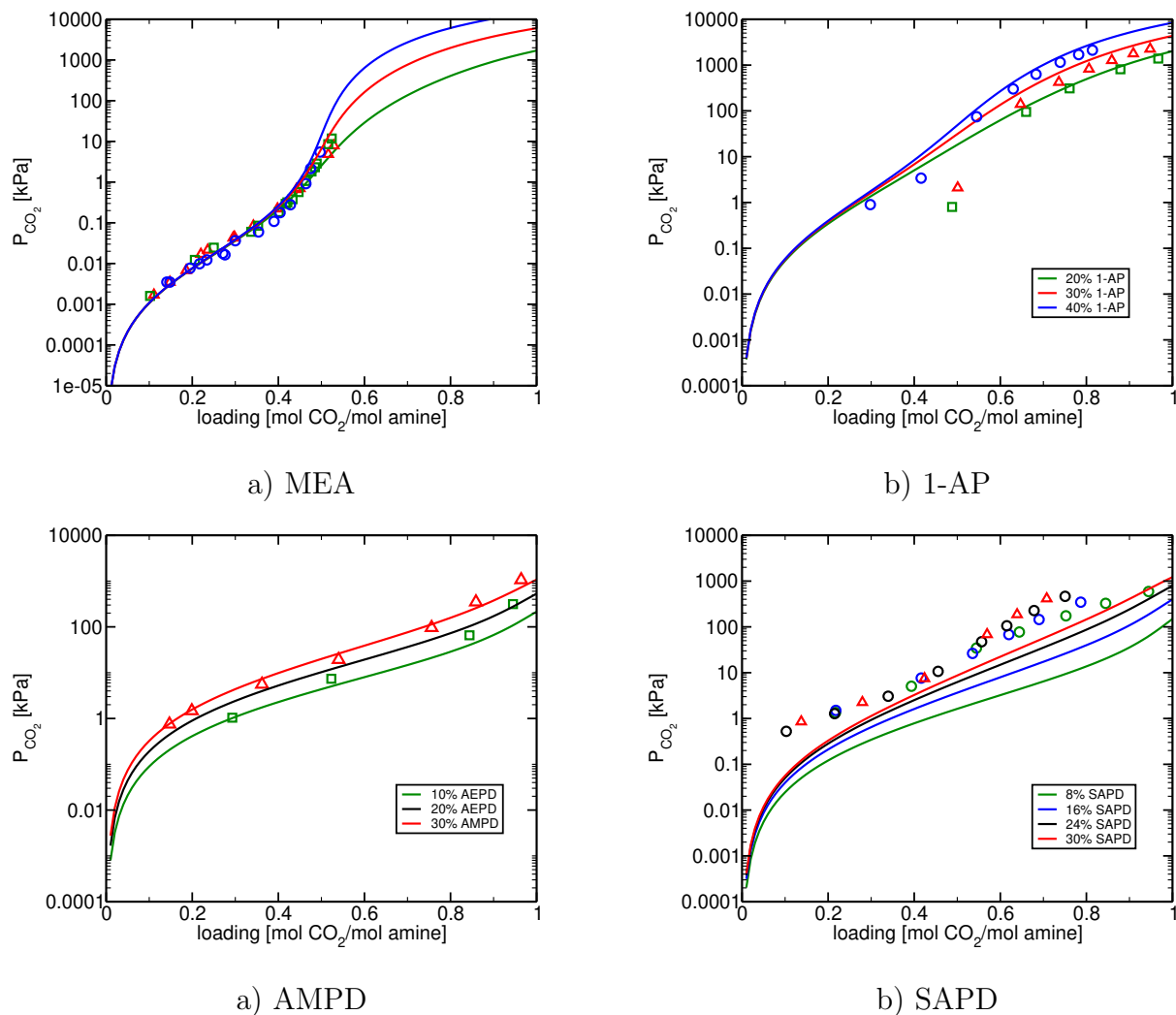


Figure 7: Effect of amine concentration on the CO<sub>2</sub> solubility of a) MEA, b) 1-AP, c) AMPD, and d) SAPD at 313.15 K. Experimental data are from references [Smith2003b](#), [Smith2003c](#), [Mathias2014](#), [Morgan2015](#), [Morgan2017](#), [Aronau2011solubility](#), [baek1998solubility](#), [78,92,94,96](#)

## 6 Uncertainty Analysis

Consideration of the effects of uncertainties in input model parameters on its outputs is a generally important aspect of modelling. [Smith2003b](#), [Smith2003c](#), [Mathias2014](#), [Morgan2015](#), [Morgan2017](#) Experimental studies often use regression models to determine fundamental thermodynamic parameters such as  $pK$  quantities shown in Tables 2 and 4. These studies do not always provide uncertainty estimates for the  $pK$  values, but when these are provided, it is in the context of a particular combined experimental and modeling approach. A reasonable indication of the uncertainty of experimentally determined

$pK$  values is the variation in the values obtained by different experimental groups using different methodologies. In a previous paper,<sup>poroozi2019efficient</sup> we provided uncertainty estimates using a molecular-based predictive methodology for values of the protonation equilibrium constant for several amines.

Uncertainty analysis in the context of a nonlinear regression model of CO<sub>2</sub> reactive absorption has recently been considered by Morgan *et al.*<sup>Morgan2015,Morgan2017</sup> by propagating the regressed model parameter uncertainties through the model to its  $P_{\text{CO}_2}$  output value. Using a previous version of the molecular-based predictive methodology of this paper, our earlier MEA study<sup>poroozi2019prediction</sup> provided uncertainty estimates for both  $P_{\text{CO}_2}$  and the solution compositions. The latter quantities are also important, but we are unaware of any other uncertainty study involving them. In this section, we provide an uncertainty analysis for both quantities for the MEA as the representative amine, and compare our results with experimental determined from different research groups.

The primary quantities used to predict  $P_{\text{CO}_2}$  and speciation concentrations in our methodology are the ideal-gas free energy changes  $\Delta G^0$  and the species hydration free energies  $\mu_i^{\text{res},\text{NVT},\infty}(T;P)$  contributing to  $pK_1$  and  $pK_2$  in Eqs. (9)–(12).<sup>eq:I00gonKdef</sup> We generated 1000 sets of  $(pK_1, pK_2)$  values from independent normal distributions with means and variances given by the indicated values in Table I,<sup>table:pKresults</sup> and for each set we solved Eqs. (I)<sup>eq:DeltaG</sup> for the resulting solution equilibrium compositions and  $P_{\text{CO}_2}$ . We then calculated the means and standard deviations of the results.

Figure 8<sup>fig:uncertainty</sup> shows representative uncertainties of our predictions for  $P_{\text{CO}_2}$  for MEA at 313.15 K (left panel), and for the MEA solution compositions (right panel) at 298.15 K. (We found no multiple sets of experimental  $P_{\text{CO}_2}$  and solution compositions at any common set of conditions.) These figures indicate that the prediction uncertainties are compatible with the scatter of the experimental results. We also found that  $pK_1$  is the most important parameter at low loadings, and that  $pK_2$  is the most important at loadings greater than 0.5, for both  $P_{\text{CO}_2}$  and the solution species concentrations.

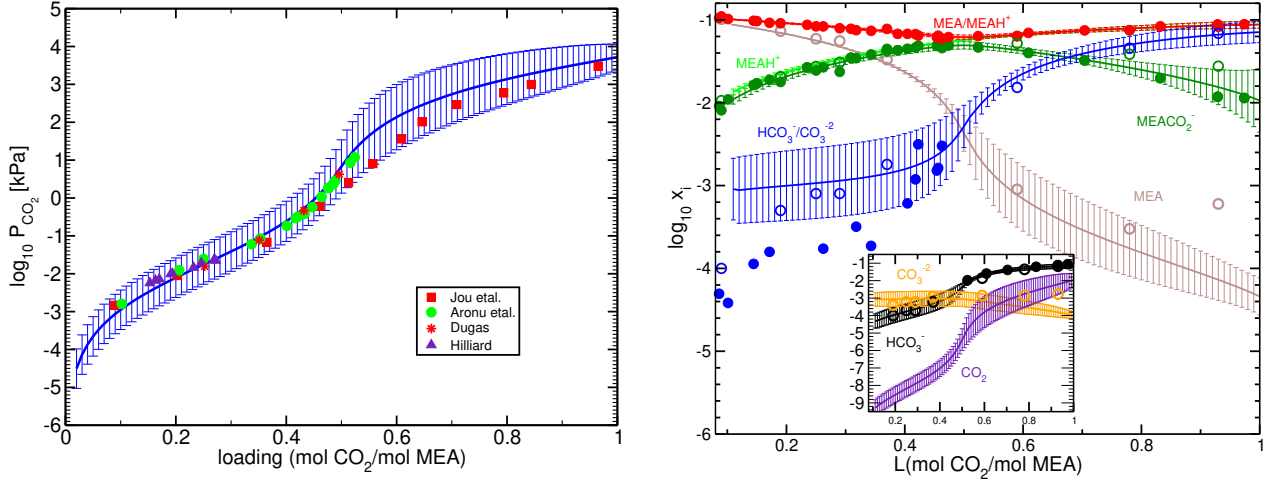


Figure 8: The left panel shows predicted values of  $P_{\text{CO}_2}$  in 30 weight % MEA at 313.15 K and their uncertainty intervals corresponding to one standard deviation. The experimental data were taken from reference [39,96,94,102]. The right panel shows the predicted solution concentrations and their one-standard-deviation uncertainty intervals for  $\text{CO}_2$  in 30 with % MEA at 298.15 K. Experimental data are same as Fig. 5.

We conclude from these figures that our predictive approach for the calculation of  $P_{\text{CO}_2}$  and the corresponding  $\text{CO}_2$ -loaded solution concentrations provides results of similar quality to those determined experimentally.

## 7 Summary and Conclusions

We have developed a methodology for predicting  $P_{\text{CO}_2}$  and the corresponding  $\text{CO}_2$ -loaded solution concentrations that requires no experimental data of any kind for the amine solvent. Our algorithm entails the calculation of ideal-gas reaction standard free energies for the two reactions (eq:R1) and (eq:R2) using quantum mechanical methodology, and the calculation of hydration free energies for the solution species using classical force field methodology and standard molecular dynamics simulations. These are used to predict  $pK_1$  and  $pK_2$ , which are incorporated within a Henry-law-based ideal solution model to predict  $P_{\text{CO}_2}$  and the solution species concentrations. We have applied our methodology to seven alkanolamine solvents, and compared our predictions with available experimental results, which have not

been obtained for some of the solvents.

We also calculated uncertainties for the predicted values of  $pK_1$ ,  $pK_2$ ,  $P_{\text{CO}_2}$  and the  $\text{CO}_2$ -loaded solution concentrations, based on propagation of the uncertainties in the ideal-gas quantities and hydration free energies through the equilibrium calculations to the final predicted quantities. We compared these with the corresponding experimental results obtained by different research groups, and inferred the experimental uncertainties from the scatter of the data. For all quantities except  $pK_1$ , we conclude that our methodology provides predictions in mutual agreement with those obtained experimentally within their mutual uncertainties. Experimental data for  $pK_1$  is generally unavailable, but we obtained it by combining our results for  $pK_1$  and  $pK_2$  with well-known experimental data for aqueous  $\text{CO}_2$  solutions to infer a value for the well-studied akanolamine protonation constant,  $pK_8$ . (Our reaction scheme avoids the use of  $\text{H}^+$  as a species, which is notoriously difficult to treat theoretically, due to the requirement to know the value of the hydration free energy of the proton as a function of temperature, an experimentally and theoretically elusive quantity.) Our results for  $pK_8$  are generally within 1  $pK$  unit of the experimental values, but we believe that the agreement could be improved by a more accurate treatment of the ideal-gas and hydration free energy properties of the protonated amine specie.

Potential improvements to our approach, which may be required for more complex solvents, would entail more accurate and precise estimates of the ideal-gas reaction free energies and of the species hydration free energies, . The recently developed (on-the-fly-polarization) OTFP methodology for calculating hydration free energies is one possibility.<sup>Kelly2020a,Kelly2020b</sup> In addition, for more complex solutions it may be necessary to account for the nonideal activity coefficient behaviour in the Henry-Law-based chemical potential model used in this paper. Although we have found this to be unnecessary for the solutions arising in the systems considered here, these may be incorporated by means of the ideal-solution chemical potential extrapolation methodology of Smith and Qi.<sup>Smith2018b</sup>

We suggest that our algorithm provides a potentially cost effective screening methodology



for improved solvent selection. Current work is under way to apply this approach to other potential solvents and their mixtures.

## 8 Acknowledgements

Financial support was provided by the Natural Science and Engineering Council of Canada (NSERC) and the Agence Nationale de la Recherche (ANR) through the International Collaborative Strategic program between Canada and France (Grant NSERC STPGP 479466-15 and ANR-12-IS09-0001-01). We thank our industrial partner, Dr. John Carroll, Gas Liquids Engineering Ltd., for supporting this research and for helpful advice and encouragement. Computational facilities of the SHARCNET (Shared Hierarchical Academic Research Computing Network) HPC consortium ([www.sharcnet.ca](http://www.sharcnet.ca)) and Compute Canada ([www.computecanada.ca](http://www.computecanada.ca)) are gratefully acknowledged.

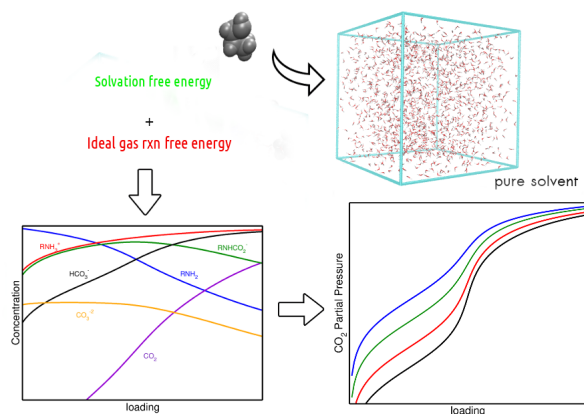


Figure 9: Graphical TOC Entry

## References

Kumoro2018

- (1) Kumoro, A. C.; Raksajati, A.; Ho, M.; Wiley, D.; Hadiyanto,; Roces, S. A.; Yung, L.; Rong, X.; Lothongkum, A. W.; Phong, M. T.; Hussain, M. A.; Daud, W. R. W.; Nam, P. T. S. Solvent Development for Post-Combustion CO<sub>2</sub> Capture: Recent Development and Opportunities. *MATEC Web of Conferences* **2018**, *156*, 03015.

- Song2018** (2) Song, C.; Liu, Q.; Ji, N.; Deng, S.; Zhao, J.; Li, Y.; Song, Y.; Li, H. Alternative pathways for efficient CO<sub>2</sub> capture by hybrid processesA review. *Renewable and Sustainable Energy Reviews* **2018**, *82*, 215–231.
- or2015amine** (3) Dutcher, B.; Fan, M.; Russell, A. G. Amine-based CO<sub>2</sub> capture technology development from the beginning of 2013: A Review. *ACS Appl. Mater. Interfaces* **2015**, *7*, 2137–2148.
- 7screening** (4) Hartono, A.; Vevelstad, S. J.; Ciftja, A.; Knuutila, H. K. Screening of strong bicarbonate forming solvents for CO<sub>2</sub> capture. *International Journal of Greenhouse Gas Control* **2017**, *58*, 201–211.
- 3efficient** (5) Barzagli, F.; Mani, F.; Peruzzini, M. Efficient CO<sub>2</sub> absorption and low temperature desorption with non-aqueous solvents based on 2-amino-2-methyl-1-propanol (AMP). *International Journal of Greenhouse Gas Control* **2013**, *16*, 217–223.
- improvement** (6) Zhang, J.; Qiao, Y.; Agar, D. W. Improvement of lipophilic-amine-based thermomorphic biphasic solvent for energy-efficient carbon capture. *Energy Procedia* **2012**, *23*, 92–101.
- evaluation** (7) Pinto, D. D.; Zaidy, S. A.; Hartono, A.; Svendsen, H. F. Evaluation of a phase change solvent for CO<sub>2</sub> capture: Absorption and desorption tests. *International Journal of Greenhouse Gas Control* **2014**, *28*, 318–327.
- choi2014co2** (8) Choi, Y.-S.; Im, J.; Jeong, J. K.; Hong, S. Y.; Jang, H. G.; Cheong, M.; Lee, J. S.; Kim, H. S. CO<sub>2</sub> absorption and desorption in an aqueous solution of heavily hindered alkanolamine: Structural elucidation of CO<sub>2</sub>-containing species. *Environmental science & technology* **2014**, *48*, 4163–4170.
- Smith1991b** (9) Smith, W. R.; Missen, R. W. *Chemical Reaction Equilibrium Analysis: Theory and Algorithms*; Krieger Publishing Co.; Reprint of same title, Willey-Interscience, 1982: Malabar, Florida, 1991.

- Mahmud2018 (10) Mahmud, N.; Benamor, A.; Nasser, M. S.; Tontiwachwuthikul, P. Carbamate Formation and Amine Protonation Constants in 2-Amino-1-ButanolCO<sub>2</sub>H<sub>2</sub>O System and Their Temperature Dependences. *J. Soln Chem.* **2018**, *47*, 262–277.
- Kamps1996 (11) Kamps, A. P.-S.; Maurer, G. Dissociation Constant of N-Methyldiethanolamine in Aqueous Solution at Temperatures from 278 K to 368 K. *J. Chem. Eng. Data* **1996**, *41*, 1505–1513.
- Rayer2014 (12) Rayer, A. V.; Sumon, K. Z.; Jaffari, L.; Henni, A. Dissociation Constants (pKa) of Tertiary and Cyclic Amines: Structural and Temperature Dependences. *J. Chem. & Eng. Data* **2014**, *59*, 3805–3813.
- Tagiuri2016 (13) Tagiuri, A.; Mohamedali, M.; Henni, A. Dissociation Constant (pKa) and Thermodynamic Properties of Some Tertiary and Cyclic Amines from (298 to 333) K. *J. Chem. & Eng. Data* **2016**, *61*, 247–254.
- Mamun2017 (14) Mamun, S.; Kamariah,; Sukirman,; Kurniawan, D.; Amelia, E.; Rahmat, V.; Alwani, D. R.; Ismadji, S.; Agustina, T. E.; Yani, I.; Komariah, L. N.; Hasyim, S. Experimental determination of monoethanolamine protonation constant and its temperature dependency. *MATEC Web of Conferences* **2017**, *101*, 02001.
- Hardsen2018 (15) Bernhardsen, I. M.; Krokvik, I. R. T.; Perinu, C.; Pinto, D. D. D.; Jens, K. J.; Knuutila, H. K. Influence of pKa on solvent performance of MAPA promoted tertiary amines. *Int. J. Greenhouse Gas Control* **2018**, *68*, 68–76.
- Nguyen2020 (16) Nguyen, W. H. C. H.; Henni, A. Dissociation Constant (pKa) and Thermodynamic Properties of 1,4-Bis(3-aminopropyl) Piperazine, 1,3-Bis(aminomethyl) Cyclohexane, Tris(2-aminoethyl) Amine, and 1-Amino-4-methyl Piperazine: Study of the Protonation Mechanism Using the Density Function Theory. *J. Chem. & Eng. Data* **2020**,
- systematic (17) McCann, N.; Phan, D.; Fernandes, D.; Maeder, M. A systematic investigation of

carbamate stability constants by  $^1\text{H}$  NMR. *International Journal of Greenhouse Gas Control* **2011**, *5*, 396–400.

- Investigations (18) Fernandes, D.; Conway, W.; Burns, R.; Lawrance, G.; Maeder, M.; Puxty, G. Investigations of primary and secondary amine carbamate stability by  $^1\text{H}$  NMR spectroscopy for post combustion capture of carbon dioxide. *J. Chem. Thermodynamics* **2012**, *54*, 183–191.
- Richner2012 (19) Richner, G.; Puxty, G. Assessing the Chemical Speciation during  $\text{CO}_2$  Absorption by Aqueous Amines Using in Situ FTIR. *Ind. & Eng. Chem. Res.* **2012**, *51*, 14317–14324.
- Gregor2018 (20) McGregor, C.; Al-Abdul-Wahid, M. S.; Robertson, V.; Cox, J. S.; Tremaine, P. R. Formation Constants and Conformational Analysis of Carbamates in Aqueous Solutions of 2-Methylpiperidine and  $\text{CO}_2$  from 283 to 313 K by NMR Spectroscopy. *J. Phys. Chem. B* **2018**, *122*, 9178–9190.
- Na2019 (21) Na, S.; June Hwang, S.; Kim, H.; Baek, I.-H.; Soon Lee, K. Modeling of  $\text{CO}_2$  solubility of an aqueous polyamine solvent for  $\text{CO}_2$  capture. *Chem. Eng. Sci.* **2019**, *204*, 140–150.
- Deshmukh1981 (22) Deshmukh, R. D.; Mather, A. E. A Mathematical Model for Equilibrium Solubility of Hydrogen Sulfide and Carbon Dioxide in Aqueous Alkanolamine Solutions. *Chem. Eng. Sci.* **1981**, *36*, 355–362.
- Najafloo2016 (23) Najafloo, A.; Feyzi, F.; Zoghi, A. T. Modeling solubility of  $\text{CO}_2$  in aqueous MDEA solution using electrolyte SAFT-HR EoS, journal = J. Taiwan Inst. Chem. Eng., volume = 58, pages = 381-390, year = 2016, type = Journal Article.
- Lloret2017 (24) Lloret, J. O.; Vega, L. F.; Llovell, F. A Consistent and Transferable Thermodynamic Model to Accurately Describe  $\text{CO}_2$  Capture with Monoethanolamine. *J. CO<sub>2</sub> Utilization* **2017**, *21*, 521–533.

- Pereira2018 (25) Pereira, L. M. C.; Vega, L. F. A systematic approach for the thermodynamic modelling of CO<sub>2</sub>-amine absorption process using molecular-based models. *Applied Energy* **2018**, *232*, 273–291.
- Wangler2018 (26) Wangler, A.; Sieder, G.; Ingram, T.; Heilig, M.; Held, C. Prediction of CO<sub>2</sub> and H<sub>2</sub>S solubility and enthalpy of absorption in reacting N-methyldiethanolamine /water systems with ePC-SAFT. *Fluid Phase Equilib.* **2018**, *461*, 15–27.
- Wang2018 (27) Wang, T.; El Ahmar, E.; Coquelet, C.; Kontogeorgis, G. M. Improvement of the PR-CPA equation of state for modelling of acid gases solubilities in aqueous alkanolamine solutions. *Fluid Phase Equilib.* **2018**, *471*, 74–87.
- Wang2019 (28) Wang, T.; Guittard, P.; Coquelet, C.; El Ahmar, E.; Baudouin, O.; Kontogeorgis, G. M. Improvement of the PR-CPA equation of state for modelling of acid gases solubilities in aqueous alkanolamine solutions. *Fluid Phase Equilib.* **2019**, *485*, 126–127.
- at2011cosmo (29) Klamt, A. The COSMO and COSMO-RS solvation models. *Wiley Interdisciplinary Reviews: Computational Molecular Science* **2011**, *1*, 699–709.
- erlach2018a (30) Gerlach, T.; Mller, S.; Smirnova, I. Development of a COSMO-RS based model for the calculation of phase equilibria in electrolyte systems. *AIChE J.* **2018**, *64*, 272–285.
- 9universal (31) Marenich, A. V.; Cramer, C. J.; Truhlar, D. G. Universal solvation model based on solute electron density and on a continuum model of the solvent defined by the bulk dielectric constant and atomic surface tensions. *J. Phys. Chem. B* **2009**, *113*, 6378–6396.
- 3carbamate (32) Gangarapu, S.; Marcelis, A. T.; Zuilhof, H. Carbamate stabilities of sterically hindered amines from quantum chemical methods: Relevance for CO<sub>2</sub> capture. *ChemPhysChem* **2013**, *14*, 3936–3943.

- heoretical
- (33) Xie, H.-B.; He, N.; Song, Z.; Chen, J.; Li, X. Theoretical investigation on the different reaction mechanisms of aqueous 2-amino-2-methyl-1-propanol and monoethanolamine with CO<sub>2</sub>. *Industrial & Engineering Chemistry Research* **2014**, *53*, 3363–3372.
- erlach2018
- (34) Gerlach, T.; Ingram, T.; Sieder, G.; Smirnova, I. Modeling the solubility of CO<sub>2</sub> in aqueous methyl diethanolamine solutions with an electrolyte model based on COSMO-RS. *Fluid Phase Equilib.* **2018**, *461*, 39–50.
- Gupta2020
- (35) Gupta, M.; Svendsen, H. F. Modeling temperature dependent and absolute carbamate stability constants of amines for CO<sub>2</sub> capture. *International Journal of Greenhouse Gas Control* **2020**, *98*.
- anishi2017
- (36) Teranishi, K.; Ishikawa, A.; Sato, H.; Nakai, H. Systematic Investigation of the Thermodynamic Properties of Amine Solvents for CO<sub>2</sub> Chemical Absorption Using the Cluster-Continuum Model. *Bull. Chem. Soc. Japan* **2017**, *90*, 451–460.
- 17modeling
- (37) Haworth, N. L.; Wang, Q.; Coote, M. L. Modeling flexible molecules in solution: A pKa Case Study. *J. Phys. Chem. A* **2017**, *121*, 5217–5225.
- ontrasting
- (38) Nakai, H.; Nishimura, Y.; Kaiho, T.; Kubota, T.; Sato, H. Contrasting mechanisms for CO<sub>2</sub> absorption and regeneration processes in aqueous amine solutions: Insights from density-functional tight-binding molecular dynamics simulations. *Chemical Physics Letters* **2016**, *647*, 127–131.
- Sakti2017a
- (39) Sakti, A. W.; Nishimura, Y.; Nakai, H. Rigorous pKa Estimation of Amine Species Using Density-Functional Tight-Binding-Based Metadynamics Simulations. *J. Chem. Theory Comput.* **2017**, *14*, 351–356.
- Sakti2017b
- (40) Sakti, A. W.; Nishimura, Y.; Sato, H.; Nakai, H. Divide-and-Conquer Density-Functional Tight-Binding Molecular Dynamics Study on the Formation of Carbamate Ions during CO<sub>2</sub> Chemical Absorption in Aqueous Amine Solution. *Bull. Chem. Soc. Japan* **2017**, *90*, 1230–1235.

- v2016first (41) Fetisov, E. O.; Kuo, I.-F. W.; Knight, C.; VandeVondele, J.; Van Voorhis, T.; Siepmann, J. I. First-Principles Monte Carlo simulations of reaction equilibria in compressed vapors. *ACS central science* **2016**, *2*, 409–415.
- balaji2015b (42) Balaji, S. P.; Gangarapu, S.; Ramdin, M.; Torres-Knoop, A.; Zuilhof, H.; Goetheer, E. L.; Dubbeldam, D.; Vlugt, T. J. Simulating the Reactions of CO<sub>2</sub> in Aqueous Monoethanolamine Solution by Reaction Ensemble Monte Carlo Using the Continuous Fractional Component Method. *J. Chem. Theory Comput.* **2015**, *11*, 2661–2669.
- fullen2018b (43) Mullen, R. G.; Corcelli, S. A.; Maginn, E. J. Reaction Ensemble Monte Carlo Simulations of CO<sub>2</sub> Absorption in the Reactive Ionic Liquid Triethyl(octyl)phosphonium 2-Cyanopyrrolide. *J Phys Chem Lett* **2018**,
- 9efficient (44) Noroozi, J.; Smith, W. R. An efficient molecular simulation methodology for chemical reaction equilibria in electrolyte solutions: Application to CO<sub>2</sub> reactive absorption. *The Journal of Physical Chemistry A* **2019**, *123*, 4074–4086.
- prediction (45) Noroozi, J.; Smith, W. R. Prediction of Alkanolamine pKa Values by Combined Molecular Dynamics Free Energy Simulations and ab Initio Calculations. *Journal of Chemical & Engineering Data* **2019**,
- Smith1994c (46) Smith, W. R.; Triska, B. The Reaction Ensemble Method for the Computer Simulation of Chemical and Phase Equilibria. I. Theory and Basic Examples. *J. Chem. Phys.* **1994**, *100*, 3019–3027.
- johnson1994 (47) Johnson, K. J.; Panagiotopoulos, Z., A.; Gubbins, K. E. A New Simulation Technique for Reacting or Associating Fluids. *Molec. Phys.* **1994**, *81*, 717–733.
- Turner2008 (48) Turner, C. H.; Brennan, J. K.; Lísal, M.; Smith, W. R.; Karl Johnson, J.; Gubbins, K. E. Simulation of Chemical Reaction Equilibria by the Reaction Ensemble Monte Carlo Method: A Review. *Molec. Simulation* **2008**, *34*, 119–146.

- Smith2018b (49) Smith, W. R.; Qi, W. Molecular Simulation of Chemical Reaction Equilibrium by Computationally Efficient Free Energy Minimization. *ACS Cent. Sci.* **2018**, *4*, 1185–1193.
- Nezbeda2016a (50) Nezbeda, I.; Moučka, F.; Smith, W. R. Recent progress in molecular simulation of aqueous electrolytes: force fields, chemical potentials and solubility. *Molec. Phys.* **2016**, *114*, 1665–1690.
- McQuarrie2000 (51) McQuarrie, D. A. *Statistical Mechanics*; University Science Books: Sausalito, California, 2000.
- thermochemistry (52) Ochterski, J. W. Thermochemistry in Gaussian. *Gaussian Inc* **2000**, *1*, 19.
- Spartan2018 (53) Spartan18, Wavefunction Inc., Irvine CA. 2018.
- Gaussian09 (54) Frisch, M. J. et al. *Gaussian 09, revision E.01*; Gaussian Inc.: Wallingford CT, 2009.
- Wang2004 (55) Wang, J.; Wolf, R. M.; Caldwell, J. W.; Kollman, P. A.; Case, D. A. Development and Testing of a General Amber Force Field. *J. Comput. Chem.* **2001**, *25*, 1157–1174.
- 6automatic (56) Wang, J.; Wang, W.; Kollman, P. A.; Case, D. A. Automatic atom type and bond type perception in molecular mechanical calculations. *Journal of molecular graphics and modelling* **2006**, *25*, 247–260.
- Bayly1993well (57) Bayly, C. I.; Cieplak, P.; Cornell, W.; Kollman, P. A. A well-behaved electrostatic potential based method using charge restraints for deriving atomic charges: the RESP model. *J. Phys. Chem.* **1993**, *97*, 10269–10280.
- 2012acpype (58) da Silva, A. W. S.; Vranken, W. F. ACPYPE-Antechamber python parser interface. *BMC research notes* **2012**, *5*, 367.
- Potoff2001 (59) Potoff, J. J.; Siepmann, J. I. Vapor-Liquid Equilibria of Mixtures Containing Alkanes, Carbon Dioxide, and Nitrogen. *AIChE J.* **2001**, *47*, 1676–1682.



- Pronk2013** (60) Pronk, S.; Pall, S.; Schulz, R.; Larsson, P.; Bjelkmar, P.; Apostolov, R.; Shirts, M. R.; Smith, J. C.; Kasson, P. M.; van der Spoel, D.; Hess, B.; Lindahl, E. GROMACS 4.5: a high-throughput and highly parallel open source molecular simulation toolkit. *Bioinformatics* **2013**, *29*, 845–854.
- Martinez2009** (61) Martinez, L.; Andrade, R.; Birgin, E. G.; Martinez, J. M. PACKMOL: a package for building initial configurations for molecular dynamics simulations. *J Comput Chem* **2009**, *30*, 2157–2164.
- Beutler1994** (62) Beutler, T. C.; Mark, A. E.; van Schaik, R. C.; Gerber, P. R.; Van Gunsteren, W. F. Avoiding singularities and numerical instabilities in free energy calculations based on molecular simulations. *Chem. Phys. Lett* **1994**, *222*, 529–539.
- Benchmarking** (63) Simmie, J. M.; Somers, K. P. Benchmarking compound methods (CBS-QB3, CBS-APNO, G3, G4, W1BD) against the active thermochemical tables: a litmus test for cost-effective molecular formation enthalpies. *The Journal of Physical Chemistry A* **2015**, *119*, 7235–7246.
- Comparison** (64) Mobley, D. L.; Dumont, E.; Chodera, J. D.; Dill, K. A. Comparison of charge models for fixed-charge force fields: small-molecule hydration free energies in explicit solvent. *The Journal of Physical Chemistry B* **2007**, *111*, 2242–2254.
- 2013partial** (65) Jämbeck, J. P.; Mocci, F.; Lyubartsev, A. P.; Laaksonen, A. Partial atomic charges and their impact on the free energy of solvation. *J. Comput. Chem.* **2013**, *34*, 187–197.
- Kroutil2017** (66) Kroutil, O.; Predota, M.; Kabelac, M. Force field parametrization of hydrogenoxalate and oxalate anions with scaled charges. *J. Mol. Modeling* **2017**, *23*, 327.
- Jensen1954** (67) Jensen, M. B.; Jorgensen, E.; Faurholt, C. Reactions between carbon dioxide and amino alcohols. I. Monoethanoamine and Diethanolamine. *Acta Chemica Scandinavica* **1954**, *8*, 1137–1140.

- ustgen1989 (68) Austgen, D. M.; Rochelle, G. T.; Peng, X.; Chen, C. C. Model of Vapor Liquid Equilibria for Aqueous Acid Gas Alkanolamine Systems Using the Electrolyte NRTL Equation. *Ind. Eng. Chem. Res.* **1989**, *28*, 1060–1073.
- equilibrium (69) Aroua, M. K.; Benamor, A.; Haji-Sulaiman, M. Z. Equilibrium Constant for Carbamate Formation from Monoethanolamine and Its Relationship with Temperature. *J. Chem. Eng. Data* **1999**, *44*, 887–891.
- 2008online (70) Böttinger, W.; Maiwald, M.; Hasse, H. Online NMR spectroscopic study of species distribution in MEA–H<sub>2</sub>O–CO<sub>2</sub> and DEA–H<sub>2</sub>O–CO<sub>2</sub>. *Fluid Phase Equilibria* **2008**, *263*, 131–143.
- Kim2009 (71) Kim, I.; Hoff, K. A.; Hessen, E. T.; Haug-Warberg, T.; Svendsen, H. F. Enthalpy of absorption of CO<sub>2</sub> with alkanolamine solutions predicted from reaction equilibrium constants. *Chem. Eng. Sci.* **2009**, *64*, 2027–2038.
- calorimetric (72) McCann, N.; Maeder, M.; Hasse, H. A calorimetric study of carbamate formation. *The Journal of Chemical Thermodynamics* **2011**, *43*, 664–669.
- experimental (73) Ciftja, A. F.; Hartono, A.; Svendsen, H. F. Experimental study on carbamate formation in the AMP–CO<sub>2</sub>–H<sub>2</sub>O system at different temperatures. *Chem. Eng. Sci.* **2014**, *107*, 317–327.
- prediction (74) Yamada, H.; Shimizu, S.; Okabe, H.; Matsuzaki, Y.; Chowdhury, F. A.; Fujioka, Y. Prediction of the basicity of aqueous amine solutions and the species distribution in the amine- H<sub>2</sub>O- CO<sub>2</sub> system using the COSMO-RS method. *Industrial & Engineering Chemistry Research* **2010**, *49*, 2449–2455.
- 2013toward (75) Conway, W.; Wang, X.; Fernandes, D.; Burns, R.; Lawrance, G.; Puxty, G.; Maeder, M. Toward the understanding of chemical absorption processes for post-combustion capture of carbon dioxide: electronic and steric considerations from the

kinetics of reactions of CO<sub>2</sub> (aq) with sterically hindered amines. *Env. Sci. & Technology* **2013**, *47*, 1163–1169.

thermodynamics

- (76) Al-Juaied, M.; Rochelle, G. T. Thermodynamics and equilibrium solubility of carbon dioxide in diglycolamine/morpholine/water. *J. Chem. & Eng. Data* **2006**, *51*, 708–717.

sterically

- (77) Sartori, G.; Savage, D. W. Sterically hindered amines for carbon dioxide removal from gases. *Ind. & Eng. Chem. Fundam.* **1983**, *22*, 239–249.

solubility

- (78) Bougie, F.; Iliuta, M. C. Solubility of CO<sub>2</sub> in and density, viscosity, and surface tension of aqueous 2-amino-1, 3-propanediol (serinol) solutions. *J. Chem. & Eng. Data* **2014**, *59*, 355–361.

Puxty2009

- (79) Puxty, G.; Rowland, R.; Allport, A.; Borwn, M.; Burns, R.; Maeder, M.; Attalla, M. Carbon Dioxide Postcombustion Capture: A Novel Screening Study of the Carbon Dioxide Absorption Performance of 76 Amines. *Environ. Sci. Technol.* **2009**, *43*, 6427–6433.

is1978vapor

- (80) Edwards, T.; Maurer, G.; Newman, J.; Prausnitz, J. Vapor-liquid equilibria in multi-component aqueous solutions of volatile weak electrolytes. *AIChE Journal* **1978**, *24*, 966–976.

Liu2019a

- (81) Liu, S.; Gao, H.; He, C.; Liang, Z. Experimental evaluation of highly efficient primary and secondary amines with lower energy by a novel method for post-combustion CO<sub>2</sub> capture. *Applied Energy* **2019**, *233–234*, 443–452.

Hamborg2009

- (82) Hamborg, E. S.; Versteeg, G. F. Dissociation Constants and Thermodynamic Properties of Amines and Alkanolamines from (293 to 353) K. *J. Chem. & Eng. Data* **2009**, *54*, 1318–1328.

- Bates1951** (83) Bates, R.; Pinching, G. D. Acidic Dissociation Constant and Related Thermodynamic Quantities for Monoethanolammonium Ion in Water From 0 to 500 C. *J. Res. Natl Bur. Stand.* **1951**, *46*, 349–352.
- Kim1987** (84) Kim, J.-H.; Dobrogowska, C.; Hepler, L. G. Thermodynamics of ionization of aqueous alkanolamines. *Can. J. Chem. Eng.* **1987**, *65*, 1726–1728.
- Antelo1984** (85) Antelo, J. M.; Arce, F.; Casado, J.; Sastre, M.; Varela, A. Protonation Constants of Mono-, Di-, and Triethanolamine. Influence of the Ionic Composition of the Medium. *J. Chem. & Eng. Data* **1984**, *29*, 10–11.
- Datta1962** (86) Datta, S. P.; Grzybowski, A. K. Acid Dissociation Constants of the Ammonium Group in 2-Aminoethanol, 2-Aminoethyl Phosphate, and 2-Aminoethyl Sulphate. *J. Chem. Soc.* **1962**, *568*, 3068–3077.
- Andes2012b** (87) Fernandes, D.; Conway, W.; Wang, X.; Burns, R.; Lawrance, G.; Maeder, M.; Puxty, G. Protonation constants and thermodynamic properties of amines for post combustion capture of CO<sub>2</sub>. *J. Chem. Thermodynamics* **2012**, *51*, 97–102.
- 2005liquid** (88) Jakobsen, J. P.; Krane, J.; Svendsen, H. F. Liquid-phase composition determination in CO<sub>2</sub>- H<sub>2</sub>O- alkanolamine systems: An NMR study. *Industrial & engineering chemistry research* **2005**, *44*, 9894–9903.
- Hilliard2008** (89) Hilliard, M. D. A Predictive Thermodynamic Model for an Aqueous Blend of Potassium Carbonate, Piperazine, and Monoethanolamine for Carbon Dioxide Capture from Flue Gas. Thesis, 2008.
- Solubility** (90) Jou, F.-Y.; Mather, A. E.; Otto, F. D. The solubility of CO<sub>2</sub> in a 30 mass percent monoethanolamine solution. *Can. J. Chem. Eng.* **1995**, *73*, 140–147.
- Solubility** (91) Martin, J. L.; Otto, F. D.; Mather, A. E. Solubility of hydrogen sulfide and carbon dioxide in a diglycolamine solution. *J. Chem. & Eng. Data* *23*, 163–164.

- |            |
|------------|
| solubility |
|------------|
- (92) Baek, J.-I.; Yoon, J.-H. Solubility of carbon dioxide in aqueous solutions of 2-amino-2-methyl-1, 3-propanediol. *J. Chem. & Eng. Data* **1998**, *43*, 635–637.
- |            |
|------------|
| solubility |
|------------|
- (93) Tong, D.; Trusler, J. M.; Maitland, G. C.; Gibbins, J.; Fennell, P. S. Solubility of carbon dioxide in aqueous solution of monoethanolamine or 2-amino-2-methyl-1-propanol: Experimental measurements and modelling. *Int. J. Greenhouse Gas Control* **2012**, *6*, 37–47.
- |            |
|------------|
| solubility |
|------------|
- (94) Aronu, U. E.; Gondal, S.; Hessen, E. T.; Haug-Warberg, T.; Hartono, A.; Hoff, K. A.; Svendsen, H. F. Solubility of CO<sub>2</sub> in 15, 30, 45 and 60 mass% MEA from 40 to 120 C and model representation using the extended UNIQUAC framework. *Chemical Engineering Science* **2011**, *66*, 6393–6406.
- |          |
|----------|
| kinetics |
|----------|
- (95) Liu, S.; Ling, H.; Gao, H.; Tontiwachwuthikul, P.; Liang, Z.; Zhang, H. Kinetics and new Brønsted correlations study of CO<sub>2</sub> absorption into primary and secondary alkanolamine with and without steric-hindrance. *Separation and Purification Technology* **2020**, *233*, 115998.
- |             |
|-------------|
| equilibrium |
|-------------|
- (96) Rebolledo-Morales, M. Á.; Rebolledo-Libreros, M. E.; Trejo, A. Equilibrium solubility of CO<sub>2</sub> in aqueous solutions of 1-amino-2-propanol as function of concentration, temperature, and pressure. *The Journal of Chemical Thermodynamics* **2011**, *43*, 690–695.
- |            |
|------------|
| Smith2003b |
|------------|
- (97) Smith, W. R.; Missen, R. W. Sensitivity analysis in ChE education. Part 1. Introduction and Application to explicit models. *Chem. Eng. Educ.* **2003**, *37*, 222–227.
- |            |
|------------|
| Smith2003c |
|------------|
- (98) Smith, W. R.; Missen, R. W. Sensitivity Analysis in ChE Education. Part 2. Application to Implicit Models. *Chem. Eng. Educ.* **2003**, *37*, 254–260.
- |             |
|-------------|
| mathias2014 |
|-------------|
- (99) Mathias, P. M.; Gilmarin, J. P. Quantitative Evaluation of the Effect of Uncertainty in Property Models on the Simulated Performance of Solvent-Based CO<sub>2</sub>-Capture. *Energy Procedia* **2014**, *63*, 1171–1185.

- Morgan2015 (100) Morgan, J. C.; Bhattacharyya, D.; Tong, C.; Miller, D. C. Uncertainty quantification of property models: Methodology and its application to CO<sub>2</sub> -loaded aqueous MEA solutions. *AIChE Journal* **2015**, *61*, 1822–1839.
- Morgan2017 (101) Morgan, J. C.; Chinen, A. S.; Omell, B.; Bhattacharyya, D.; Tong, C.; Miller, D. C. Thermodynamic modeling and uncertainty quantification of CO<sub>2</sub> -loaded aqueous MEA solutions. *Chem. Eng. Sci.* **2017**, *168*, 309–324.
- 2009carbon (102) Dugas, R. E. Carbon dioxide absorption, desorption, and diffusion in aqueous piperazine and monoethanolamine. **2009**,
- Kelly2020a (103) Kelly, B.; Smith, W. R. Alchemical hydration free-energy calculations using molecular dynamics with explicit polarization and induced polarity decoupling: an On-the-Fly polarization approach. *J. Chem. Theory Comput.* **2020**, *16*, 1146–1161.
- Kelly2020b (104) Kelly, B.; Smith, W. R. A Simple Method for Incorporating Polarization Effects in Solvation Free Energy Calculations Using Fixed-Charge Force Fields. *ACS Omega* **2020**, <https://dx.doi.org/10.1021/acsomega.0c01148>.